UNITED AIRCRAFT CORPORATION

United Aircraft Research Laboratories

EAST HARTFORD, CONNECTICUT

United Aircraft Research Laboratories

UNITED AIRCRAFT CORPORATION

EAST HARTFORD, CONNECTICUT

Report H-910091-21

Exploratory Experimental Study of the Effects of Inlet Conditions on the Flow and Containment Characteristics of Coaxial Flows

NASA Contract No. NASw-847

REPORTED BY Bruce V. Johnson
Bruce V. Johnson

APPROVED BY Robert E. Olson
Robert E. Olson, Chief
Gas Dynamics Section

DATE September 1969

NO. OF PAGES 47

COPY NO. ________

FOREWORD

An exploratory experimental and theoretical investigation of gaseous nuclear rocket technology is being conducted by the United Aircraft Research Laboratories under Contract NASw-847 with the joint AEC-NASA Space Nuclear Propulsion Office. The Technical Supervisor of the Contract for NASA is Captain C. E. Franklin (USAF). Results of portions of the investigation conducted during the period between September 15, 1968 and September 15, 1969 are described in the following five reports (including the present report) which comprise the required ninth Interim Summary Technical Report under the Contract:

1. Roman, W. C., J. F. Klein, and P. G. Vogt: Experimental Investigations to Simulate the Thermal Environment, Transparent Walls and Propellant Heating in a Nuclear Light Bulb Engine. United Aircraft Research Laboratories Report H-910091-19, September 1969.

2. Mensing, A. E. and J. F. Jaminet: Experimental Investigations of Heavy-Gas Containment in R-F Heated and Unheated Two-Component Vortexes. United Aircraft Research Laboratories Report H-910091-20, September 1969.

3. Krascella, N. L.: Theoretical Investigation of the Radiant Emission Spectrum from the Fuel Region of a Nuclear Light Bulb Engine. United Aircraft Research Laboratories Report H-910092-12, September 1969.

4. Latham, T. S., H. E. Bauer, and R. J. Rodgers: Studies of Nuclear Light Bulb Start-up Conditions and Engine Dynamics. United Aircraft Research Laboratories Report H-910375-4, September 1969.

5. Johnson, B. V.: Exploratory Experimental Study of the Effects of Inlet Conditions on the Flow and Containment Characteristics of Coaxial Flows. United Aircraft Research Laboratories Report H-910091-21, September 1969. (present report)

Report H-910091-21

Exploratory Experimental Study of the Effects of Inlet Conditions on the Flow and Containment Characteristics of Coaxial Flows

TABLE OF CONTENTS

TABLE OF CONTENTS (Continued)

Report H-910091-21

Exploratory Experimental Study of the Effects of Inlet Conditions on the Flow and Containment Characteristics of Coaxial Flows

SUMMARY

Fluid mechanics experiments were performed to investigate the factors which influence the formation and growth of the large eddy structure in developing coaxial shear flows. Information from these experiments was used to develop inlet configurations and inlet flow conditions in order to improve containment of the inner-jet gas for application to the open-cycle gaseous-core nuclear rockets and to improve film cooling flow characteristics for application to closed-cycle nuclear light bulb rockets.

The tests were performed in a 10-in.-dia chamber with lengths of 10 in. and 30 in. The inlet to the chamber had provision for two- or three-stream operation. Air or Freon-11 was used for the inner-jet gas, and air was used for the buffer-stream gas (if used) and outer-stream gas. Flow visualization was obtained by coloring the inner-jet gas with iodine gas and photographing the flow with high-speed motion pictures. Hot-wire and pitot probes were used to obtain average and fluctuating velocity data in the chamber. Film-cooling flow visualization tests were also performed with a 5-in.-dia cylinder in the center of the 10-in.-dia chamber.

The results from these tests indicate that the large eddies, characteristic of the interface between coaxial flows, could be essentially eliminated for flows in short chambers. This was done by decreasing the velocity gradient between the two streams at the coaxial-flow inlet so that any disturbances in the system would be convected from the chamber before developing into large waves or eddies. The best apparent inner-jet gas containment obtained with a modified inlet configuration in the short chamber was better than was obtained from previous tests. Tests with the centerbody and 30-in.-length configuration indicated that the disturbances from both the inlet and the exhaust systems need to be damped to prevent noticeable waves from forming in the chamber and developing into eddies.

RESULTS

1. The large-eddy disturbances which occurred in previous UARL coaxial-jet tests with discontinuous-inlet-velocity profiles were essentially eliminated by the use of a porous material upstream of the inlet plane to smooth out the inlet velocity profiles. Use of these materials also decreased the rms axial velocity fluctuations from 40 percent to approximately 7 percent in the test chamber near the inlet plane.

2. The apparent inner-jet gas containment obtained with the modified porous-material inlets was considerably improved over that obtained in previous tests. With Freon-11 as the inner-jet gas, the containment at a ratio of outer-stream flow rate to inner-jet flow rate of 25 was twice that for previous UARL tests.

3. For tests with coaxial streams of approximately equal velocity and porous material inlets, the addition of a centerbody which created annular coaxial flow resulted in decreased turble size and decreased mixing between the two streams. For these tests, insertion of porous material at the exhaust plane resulted in flow without any apparent wave disturbances or turbles for the entire test chamber length.

4. The large-eddy disturbances observed in present and previous UARL coaxial-flow tests have a range of disturbance frequencies rather than a single eddy shedding frequency.

5. Wave disturbances observed in coaxial flows with porous-material inlets occurred most often at frequencies less than those for which 2-D inviscid theory predicted the largest wave growth factor.

INTRODUCTION

The goal of developing a gaseous-core nuclear rocket engine is desirable because the potential specific impulse obtainable is high (between 1500 and 3000 sec) and because the potential engine thrust-to-weight ratio is greater than one. Because of this potential, analytical and experimental studies to determine the feasibility of open-cycle and closed-cycle versions of the gaseous-core nuclear rocket have been conducted at the United Aircraft Research Laboratories and elsewhere since approximately 1959.

In the current open-cycle concepts the nuclear fuel and propellant are injected into the reactor chamber at different locations and exhausted together from the reactor chamber through the nozzle. The energy generated from nuclear fissions in the gaseous fuel is transferred to the propellant by thermal radiation. For the open-cycle engines, the fluid mechanics requirements are that (1) a large fraction of the reactor chamber be filled with gaseous nuclear fuel, and (2) the ratio of the propellant weight flow rate to the gaseous nuclear fuel weight flow rate be large.

In the closed-cycle, or nuclear light bulb concept, the gaseous fissioning fuel is separated from the seeded hydrogen propellant by an internally cooled transparent wall through which heat is transferred by thermal radiation. This concept is attractive because the physical barrier between the fuel and propellant offers the possibility of perfect containment of fuel and fission products. A major fluid mechanics requirement for the nuclear light bulb concept is that the transparent wall be protected from the heated propellant and nuclear fuel by a coolant gas film.

Background Information for Coaxial-Flow Applications to the Open-Cycle Concept

Studies to determine the feasibility of an open-cycle coaxial-flow gaseous-core nuclear rocket have been conducted at and directed from Lewis Research Center for several years. The coaxial-flow concept was outlined in Ref. 1 and the status of the work at Lewis Research Center and elsewhere has been summarized in Refs. 2 and 3. A sketch of the coaxial-flow gaseous-core nuclear rocket engine showing the fuel-containment region, propellant region, and flow direction is shown in Fig. 1. Most of the experimental work done thus far, including the research reported herein, has been directed toward simulating the flow from plane A-A to the exhaust nozzle.

In a previous coaxial flow study (Ref. 4), the containment characteristics of one-, two-, and three-component coaxial jets in short chambers were investigated. For many flow conditions, the interface between the inner-jet gas and outer-stream gas was found to oscillate in waves or large eddies that grew in size as the flow progressed from the inlet to the exhaust. These large-scale eddies would be undesirable in a full-scale reactor since they promote a large amount of mixing between the simulated fuel and propellant.

The objectives for this phase of the program were (1) to investigate the factors which influence the formation and growth of the large eddy structure in developing coaxial flows and (2) to develop inlet configurations which will result in improved performance of the coaxial-flow region of the open-cycle reactor.

Background Information for Coaxial-Flow Applications to the Closed-Cycle Concept

Studies to determine the feasibility of the nuclear light bulb engine have been conducted at UARL for several years. In a study of a specific engine (Ref. 5), the geometry, materials, gases, and gas flow rates that would be compatible for a full-scale reactor were specified. The film cooling requirements, deduced from Ref. 5 for the maintenance of a satisfactory temperature on the propellant-flow side of the transparent wall, require better performance than has been obtained to date in conventional film cooling tests. A typical cavity length is 6 ft with a propellant injection slot height of 0.121 ft. Approximate wall temperature and fluid mechanic constraints require that the film effectiveness be maintained above 90 percent and that not more than 20 percent of the inlet slot height be for film cooling gases. The ratio of wall length to slot height which must be effectively cooled is on the order of 240.

Film cooling studies by Chin, et al., (Ref. 6), Seban (Ref. 7), and Kacker and Whitelaw (Ref. 8) indicate the maximum ratio of wall length to slot height for which 90 percent film effectiveness could be achieved were 10, 20, and 40, respectively. For these tests, the boundary layers upstream and downstream of the coolant injection slot were turbulent. For the nuclear light bulb engine, the flow velocities and Reynolds numbers are expected to be low enough so that high film effectiveness can be achieved over much greater distance providing the formation of a large eddy structure leading to natural boundary layer transition does not occur.

The objectives for this phase of the program were (1) to investigate the factors which influence the formation and growth of the large eddy structure in developing coaxial flows of approximately equal velocities and (2) to develop configurations which will result in improved film cooling effectiveness.

DESCRIPTION OF TEST EQUIPMENT AND PROCEDURES

Equipment

Flow System

A schematic of the test apparatus and a photograph of the test facility is shown in Figs. 2 and 3, respectively. Separate plenums supplied three streams to the chamber which were denoted the inner jet, the buffer stream, and the outer stream. The gases flowed from the plenums through a specific inlet configuration to a specific chamber configuration employed in a test. The flow was exhausted from the lower end of the chamber. To supply the desired combinations of inner-jet, buffer-stream, and outer-stream gases and inlet gas velocities to the inlet manifold, a combination of gas generators, heaters, and compressors were used. Air flow for the outer stream and buffer stream at rates up to 1.5 lb/sec was drawn into the chamber using the Research Laboratories vacuum system. The flow rates for the combined outer and buffer streams was measured with a nozzle not shown in Fig. 3. The buffer-stream and inner-jet gas flow rates were measured with the variable area flowmeters shown in the photograph. For the flow visualization tests, the outer-stream and buffer-stream air was heated to approximately 260 deg F using the "light-gas" supply system described in Ref. 9. The inner-jet gases used were air and Freon-11. The air was obtained from the 400 psi air supply and heated to 260 deg F in a conventional tube-and-shell heat exchanger. The Freon-11 was vaporized in the shell side of a tube-and-shell heat exchanger and superheated in the air superheater. For the average velocity and turbulence measurements, unheated air was used for all the streams.

Chamber and Inlet Configurations

Sketches of the chamber configurations employed during the tests are shown in Fig. 4. The chambers were constructed of transparent uncolored cast acrylic tubes and had an inside diameter of 10 in. for all tests. The short chamber (Fig. 4a) with an exhaust nozzle diameter of 6 in. is the same configuration employed in Ref. 4. The long chamber (Fig. 4b) has the same exhaust nozzle as the short chamber but a 33 in. length from the inlet plane to the nozzle throat compared to 10 in. for the short chamber. The annular chamber with open exhaust (Fig. 4c) has a 2.5 in. annulus between a 5-in.-dia cylindrical centerbody and the 10-in.-ID chamber wall. The exhaust for this configuration has a conical transition from the chamber wall dia to the 8-in.-dia vacuum duct. The annular chamber with foam exhaust (Fig. 4d) has the same centerbody used for the previous configuration. A 1/2-in.-thick foam layer, fastened to a porous plate, was installed at the exhaust to decrease the pressure fluctuations in the chamber resulting from flow disturbances in the exhaust system.

Sketches of the inlet configurations employed during the tests are shown in Fig. 5. The screen inlet (Fig. 5a) was that employed in Ref. 4. The foam inlet (Fig. 5b) was constructed to obtain a smooth inlet velocity profile with a moderate maximum velocity gradient between the outer stream and the inner jet. The foam and perforated plate inlet (Fig. 5c) is a modification to the foam inlet, developed late in the study, to eliminate the radial inflow of the outer-stream gas past the inner-jet radius, r_I. For both the foam inlet and the foam and perforated plate inlet, no gas was injected from the buffer plenum; however, the outer-stream gas did flow radially inward in the foam from the porous plate to the chamber inlet plane for both inlets. The annular foam inlet (Fig. 5d) was used for tests in the annular chamber with open exhaust (Fig. 4c) and with foam exhaust (Fig. 4d). The construction was similar to the foam inlet (Fig. 5b).

Experimental Techniques

Flow Visualization

A schematic of the optical system used for flow visualization photography is shown in Fig. 6. Light was supplied by quartz-iodine lamps and diffused with frosted glass or drawing vellum to provide a uniform background illumination. Iodine was used for coloring the inner-jet gas for all of the flow visualization tests. Kodak Ektachrome film type 4241EF for high-speed cameras was used for all the motion pictures obtained. Most of the film sequences were obtained with a Fastax camera at 1000 frames per second.

Velocity and Turbulence Measurements

A DISA hot-wire anemometer model 55D01 with a type 55A36 miniature hot-wire probe was used to obtain the hot wire average velocity measurements and the turbulence intensity measurements. Hot-wire calibrations were performed before and after each run (flow case) to ensure that the calibration remained constant during the run. The turbulence intensity measurements were interpreted using the standard techniques outlined in the equipment manual (Ref. 10).

Velocity measurements were also obtained with a three-hole cobra probe. The probe was calibrated for $\Delta P/\rho V^2$, where ΔP is the difference between the total pressure and the pressure measured by the taps when the probe was aligned with the flow. This probe was used because the static pressure varies radially and axially and a local velocity measurement was desired. The gas density used to interpret data was calculated from the measured chamber pressure and the average of the inner-jet, buffer-stream, and outer-stream inlet gas temperatures which varied less than 10 deg F.

Calculation of Inner-Jet Gas Containment

An apparent inner-jet gas containment volume was obtained from the flow-visualization high-speed motion pictures. A single frame was chosen to be representative of the flow and magnified with a projector to obtain the outline of the chamber and the dense inner-jet gas volume. The ratio of the apparent average partial pressure of the inner-jet gas to the total pressure was calculated for each case from the following equation:

$$\frac{\overline{P_I}}{P} = \frac{1}{L_c r_o^2} \int_0^{L_c} r^{*2} \, dz$$

where r* is the outer radius of the dense inner-jet gas.

DISCUSSION OF FLOW CHARACTERISTICS IN SHORT CHAMBERS

Turbulence and Wave Disturbance Characteristics with Screen Inlets

Hot-wire data and wave disturbance data were obtained to determine the nature and origin of the fluctuating flow characteristics reported in Ref. 4. The pertinent information obtained for the short chamber and screen-inlet configuration is presented in Figs. 7 and 8 for flows with approximately equal velocities and with a velocity ratio of two, respectively. High-speed motion pictures were used to obtain wave disturbance data from flow visualization tests. Visual analysis of the motion picture film was made to determine the length of time or number of frames between large waves or turbles in the flow. A disturbance frequency for the single turble was defined to be the quotient of the number of frames per second, N, divided by the number of frames between the waves, ΔN. The percentage of waves in a disturbance frequency band was determined and plotted. The hot-wire rms voltage fluctuation spectrum was measured at two axial locations for r = 2.5 in.; i.e., the radial location where the largest waves appear. These hot-wire measurements were for the streamwise fluctuating component. For the two flow conditions, the spectral data does not show an increase in the rms voltage fluctuations at the frequencies having the largest number of large scale turbles. For the spectral data of case 6, shown in Fig. 8, the largest fluctuations occurred at 50 cps which is approximately 1/3 the most frequently observed wave disturbance frequency. From these data, it was concluded that the main source of streamwise velocity fluctuations for the screen-inlet configuration at this radial location was not from the large-scale waves observed. Measurements from Ref. 15 indicate the cross-stream fluctuation velocity component is larger for waves than the streamwise fluctuation velocity component. Future measurements of wave characteristics should probably center on the cross-stream velocity fluctuations rather than the streamwise fluctuations.

In addition to the spectral measurements, turbulent intensity data for the streamwise velocity fluctuations were also measured at 1/2-in. radial intervals for 4 axial locations. These data are presented in Fig. 9a. At Z = 1 in., the turbulent wakes from the plenum walls at r = 2.5 in. and r = 3.25 in. provide the largest turbulent intensity levels. The turbulent intensities decay with increasing distance from the inlet plane. For this flow condition, the turbulent intensity remained greater than 0.1 for $r > 3.5$ at all stations. For $r \leq 4.0$ in., the fluctuations are probably from the flow through the screen. These fluctuations are decaying faster than those in the shear region and the inner-jet region probably because the scale of turbulence is small due to screen grid size. The conclusions from these tests were that the relatively large wakes from the inlet manifold plenum walls was creating more turbulence than the developing waves for $V_{BAO}/V_I \approx 1$ and that the large velocity gradients were causing the large eddies to form very close to the inlet for $V_{BAO}/V_I > 1$.

A second screen inlet was assembled identical to that shown in Fig. 5a except that no sealant was used between the plenums so that the plenum wall thickness was less than 0.030 in. Root-mean-square turbulent fluctuation levels were obtained for velocity ratios, V_{BAO}/V_I, equal to approximately 1, 2, and 4. For $V_{BAO}/V_I \approx 1$, the wake from the plenum wall was effectively eliminated. The turbulent intensity level near the inlet was 10 to 20 percent (z = 1.0 in.), which is lower than the maximum values of 50 percent measured in previous tests but was higher than desired. For $V_{BAO}/V_I \approx 2$, the velocity profile obtained from hot-wire measurements between the inner jet and outer stream also indicated the absence of any wake from the plenum divider. The turbulence levels at r = 2.5 in. had a maximum value of 50 percent for z = 0.5 in., and decreased with increasing distance from the inlet. For $V_{BAO}/V_I \approx 4$, the local turbulent level and local hot-wire power dissipation distribution increased and decreased, respectively, with increasing distance from the inlet plane; this may indicate the formation of a recirculation cell. The turbulent intensity distribution in the short chamber with the screen inlet is similar to that reported by Weinstein, et al., in Refs. 11, 12, and 13, for flow in an 8-in.-sq duct downstream of a 3/4-in.-dia thin-wall tube and in a 6-in.-dia duct downstream of a 2.8-in.-dia thin-wall tube.

Turbulence and Wave Disturbance Characteristics with Foam Inlets

Undesirable characteristics of the flow from the screen inlet were (1) the sharp slope of the velocity profile between the inner jet, the buffer stream, and the outer stream and (2) the relatively high turbulent level downstream of the screen inlet. Theoretical studies (Ref. 14) on spatially growing disturbances in an inviscid shear layer indicate the distance required for large eddies to develop is proportional to the shear layer width. Experimental studies on transition in a separated laminar boundary layer (Ref. 15) support results from the theoretical analysis of Ref. 14 and indicate the influence of the disturbance pressure levels on the size of the wave or eddies a given distance from the origin of the flow. Because of the influence of shear layer thickness on the eddy development length, increasing the shear layer width from the small distance between the plenum (Ref. 4) to a moderate fraction of the chamber radius should cause the large eddy development length to increase. Allowing the flow to pass through a porous media with a moderate pressure drop (i.e., approximately 10 to 20 $\rho V^2/2$) will permit some of the discontinuities that occur at the plenum wall to be removed. In addition, the velocity profile gradient should be decreased, depending on the uniformity of the porous media. Scott industrial foam, used in the research on atmospheric flow systems reported in Ref. 16, appeared to have these characteristics. A layer of foam 1 in. thick with the manufacturers identification of 30 PPI was fastened with adhesive to a porous plate for the first series of tests, as shown in Fig. 5b.

The turbulent intensity distribution presented in Fig. 9b shows that the turbulent intensity was greatly reduced in the central portion of the chamber compared to the results obtained from tests with the screen inlet shown in Fig. 9a. The turbulent intensity downstream of the inlet is less than 0.08 for most locations and, for this flow condition, decays with increasing distance from the inlet. For other flow conditions with high velocity ratios, i.e., $V_{BAO}/V_I = 5$, the turbulent intensity increased, indicating the production of turbulent energy downstream of the inlet from the mixing process.

The high-speed motion-picture sequences presented in Fig. 10 for tests with the screen inlet, the foam inlet, and the foam and perforated plate inlet show the effect of inlet flow conditions on the wave disturbance characteristics for velocity ratios, $V_{BAO}/V_I > 15$. These flow rate ratios with Freon-11 as the inner-jet gas are the same order of magnitude as envisioned for the full-scale flow reactor. For cases 9013 and 9014 (Ref. 4) the large-scale eddies, deemed undesirable, are present. For case 79 the large-scale eddies do not occur but small amplitude waves, not noticeable in these film sequences, do occur. Although the flow fluctuations for case 79 are essentially eliminated, the containment volume is low because radial flow within the foam layer caused the inner-jet to contract. This contraction decreased the indicated velocity ratio, decreased the inner-jet inlet area to less than 15 percent of the chamber cross-sectional area, and limited the obtainable containment volume. To improve the containment characteristics, the foam inlet was modified by extending the inner-jet plenum to the inlet plane and removing the foam for $r < r_I$ (fig. 5c). For case 124 (Fig. 10d), small eddies, similar to those previously observed in Figs. 10a and 10b, appeared and grew with increasing distance from the inlet plane. However, the containment was improved as will be shown in a later section.

The wave disturbance spectrum obtained from high-speed motion pictures is shown in Fig. 11 for tests with air and Freon-11 as the inner-jet gases. The percent of the waves for each frequency range is presented as a function of the normalized disturbance frequency. The disturbance frequency was previously defined as the quotient of the number of frames per sec divided by the number of frames between waves. The velocity shear layer momentum thickness, θ, defined in a two-dimensional manner, and the approximate maximum velocity in the chamber, V*, were used to obtain the normalized disturbance frequency, $(2\theta N)/(V^*\Delta N)$, which is a form of the Strouhal number. For tests with Freon-11 as the inner-jet gas, the distribution of waves in each normalized disturbance frequency band appears to be independent of the inner-jet gas flow rate (Fig. 11b). The curve is skewed rather than being Gaussian about a single frequency. The shape is similar to those presented in Figs. 7 and 8 for tests with the screen inlets. For tests with air as the inner-jet gas, the trend is about the same as with Freon-11; however, the scatter of the data is greater and there appears to be a slight influence of the weight flow ratio. The data for the lowest weight flow rates occur at slightly higher normalized frequencies than those those at the higher weight flow ratios. A limited amount of data for tests with $V_{BAO} \approx 34$ ft/sec and air as the inner-jet gas indicates the most frequent disturbance was shifted to a higher normalized disturbance frequency than was shown in Fig. 11 for tests with $V_{BAO} \approx 80$ ft/sec.

The theoretical growth factors for a two-dimensional hyperbolic tangent velocity profile from Ref. 14 are shown in Fig. 12a. The spatial growth factor is that calculated for a single small-amplitude wave at a specific cyclic frequency. In order to qualitatively compare the present experimental results with the theoretical results, an experimental wave disturbance cyclic frequency was defined as 2 π times the normalized disturbance frequency, $(N\ 2\theta)/(\Delta NV^*)$. For the hyperbolic tangent velocity profile, $V = (V_O/2)(1 + \tanh y/L)$, θ is equal to L/2. The average experimental disturbance spectrum for tests with air and Freon-11 as the inner-jet gases is shown in Fig. 12b as the variation of the percent of waves in an indicated cyclic frequency band with the disturbance cyclic frequency. These average results for air and Freon-11 are essentially the same within the accuracy of these measurements. Note that the cyclic frequency at which most waves occur is less than one half the cyclic frequency at which 2-d waves have the maximum growth rate. If the disturbances were of equal strength, the strongest waves at the exit should be those with the largest spacial growth factor. One reason that the trends do not agree may be that the spacial growth factor is influenced by the axisymmetric nature of the problem. The high-frequency, short-wavelength disturbances may not occur as axisymmetric waves but may rather be three-dimensional in nature and are not seen as well defined waves. A second reason may be that the pressure disturbances from the exhaust system feeding to the chamber through the exhaust nozzle are not uniform at all cyclic frequencies and, hence, any amplification of a strong disturbance will be seen before a larger amplification of a very weak disturbance.

The conclusion from these and other exploratory tests is that the formation of large scale eddies can be delayed by tailoring the inlet flow conditions.

Velocity Measurements with Foam Inlets

Velocity measurements were obtained at several locations in the chamber to evaluate the average flow characteristics obtained with the foam inlets. Pitot probe and hot-wire probe data were obtained from tests employing the short chamber (Fig. 4a) and 1/2-in. foam inlet (Fig. 5b) configuration at several axial locations, at several inlet velocities, and for V_{BAO} values of approximately 80 and 34 ft/sec. A comparison of velocity profiles obtained for V_O = 93.6 ft/sec and $V_B = V_I = 0$ with hot-wire and pitot probes for the same configuration and flow conditions but at different azimuthal locations is shown in Fig. 13. The profiles have small irregularities which reflect the flow characteristics rather than velocity measurement errors. These are due to the nonaxisymmetry of the porous plate backing (i.e., hexagonal arrangement of holes). The differences between the two profiles may be due to the nonaxisymmetry of the porous plate backing and nonuniformities in the foam. The pitot probe measurements are inaccurate at velocities less than 20 ft/sec. Therefore, velocities were determined from the hot-wire measurements for the low-velocity region and indicate that velocities less than one ft/sec were obtained for $r < 2.0$ in. This indicates that gas injected at $r_B = 3.25$ in. was flowing radially inward in the foam from that location to $r = 2.0$ in.

Typical profiles are shown in Fig. 14 for $V_{BAO} \approx 80$ ft/sec and in Fig. 15 for $V_{BAO} \approx 34$ ft/sec at several values of V_I. The axial velocities from $r = 0$ to $r = 2.0$ in. were approximately equal to V_I. From $r = 2.0$ in. to $r = 4.0$ in. the velocity increased to a value greater than V_{BAO} but less than V_O except for case 61 shown in Fig. 15. For this case, gas from both the inner-jet region and the outer-stream region flowed into the buffer-stream region as shown by the velocity decrease at $r = 2.75$ in. These results show that the desired low velocities downstream of the inner jet and high velocities near the outer wall were obtained with the desired gradual velocity profile between these two regions.

Velocity profiles were obtained with a hot-wire probe at several axial locations for $V_{BAO}/V_I = 27$ and $V_{BAO} = 80$ ft/sec and are shown in Fig. 16. The local velocities at $z = 1.0$ in. and 3.5 in. for $r \leq 2.0$ in. are close to the inner-jet injection velocity, V_I. At $Z = 6.0$ in. the effect of the converging exhaust nozzle was felt by the inner-jet gas as it was accelerated from the chamber. The velocity profiles were integrated from $r = 0$ to obtain the approximate location for the outermost streamline from the inner jet. These locations, also shown in the figure, are in good agreement with the high-speed motion-picture flow visualization data which indicate the outer radius of the densely colored inner-jet gas. From this comparison, it was concluded that the motion pictures could be used to determine the approximate inner-jet gas containment.

DISCUSSION OF FLOW CHARACTERISTICS IN LONG CHAMBERS

Three series of tests were conducted to determine the conditions required to delay the formation of large-scale eddies between coaxial streams at approximately equal velocities for application to the nuclear-light-bulb film cooling problems. The first series of tests was conducted employing the long chamber (Fig. 4b) and 1/2-in. foam inlet with $r_I/r_O = 0.5$ and $r_B/r_O = 0.65$ (Fig. 5b). For these tests, the buffer-stream and outer-stream velocities were approximately the same. For flow conditions when the velocity ratio, V_O/V_I, was between one and two, axisymmetric waves between the inner jet and buffer stream were observed at ratios of z/D greater than approximately one and eddies appeared to form at ratios of z/D greater than approximately two. The scale of these eddies was approximately 0.1 r_o, whereas the scale of the eddies with the screen inlet was approximately 0.3 r_o. A typical high-speed motion picture frame showing these waves and turbles is shown in Fig. 17a for $V_O/V_I = 1.22$.

The second series of tests was conducted employing the annular chamber with open exhaust (Fig. 4c) and the 1/2-in. annular foam inlet (Fig. 5d) with $r_I/r_o = 0.60$. Flow visualization with high-speed motion pictures was obtained for six flow conditions with V_o/V_I equal to 0.55, 0.81, 0.85, 0.90, 1.04, and 1.26. Thus, the stream velocities were never perfectly matched; however, the irregularities in the inlet velocity profiles are probably greater than the 4 percent minimum velocity ratio difference. For all of these tests, axisymmetric waves occurred at values of z/D greater than two (Fig. 17b). For flow conditions with the larger velocity differences between V_O and V_I, the waves appeared to roll up at $z/D \approx 3$ (i.e., end of chamber). These waves are not obvious on a single motion picture frame such as shown in Fig. 17b due to the relatively small size of waves and the inner stream width compared to the chamber diameter. However, the waves can be easily seen when the high-speed color motion pictures, obtained at 1000 frames per second, are projected at 24 frames per second. Some nonaxisymmetric waves were observed in the flow and were probably due to asymmetries in the inlet. From subsequent tests described in the next paragraph it was concluded that the disturbances which led to the formation of large-scale eddies originated in the exhaust system.

A third series of tests was conducted employing the annular chamber with foam exhaust (Fig. 4d) and 1/2-in. annular foam inlet with $r_I/r_O = 0.65$ (Fig. 5d). For these tests, no waves or disturbances were observed in the high-speed motion pictures for velocity ratios V_O/V_I between 0.5 and 2.0. A typical frame from these movies is shown in Fig. 17c for $V_O/V_I = 1.13$. Increasing the velocity ratio V_O/V_I to 4 caused the inner stream to thin but no waves appeared. After the motion pictures were obtained, a slightly deformed cylinder was introduced as the centerbody. The flows observed with $0.8 < V_O/V_I < 1.5$ and this nonaxisymmetric centerbody did not appear to have any waves or eddies.

The conclusion from these series of tests in the L/D = 3 chambers was that, for the conditions investigated, the amplitude of the large axisymmetric waves and eddies could be decreased with the addition of a centerbody and could be essentially eliminated with the introduction of a foam exhaust to damp the fluctuations from the exhaust system.

DISCUSSION OF CONTAINMENT CHARACTERISTICS IN SHORT CHAMBERS

Flow visualization tests were conducted to determine the apparent containment characteristics obtained in the short chamber with the foam inlet and the foam and porous plate inlet. These results were compared to data from Ref. 4 and to the requirements for open-cycle gaseous-core rockets outlined in Ref. 2.

Containment with Foam Inlets

Individual frames from high-speed motion pictures were visually observed to determine the approximate inner-jet gas contained in the short chamber (Fig. 4a) for a given test. Motion pictures were obtained for tests employing the foam inlet (Fig. 5b) with air and Freon-11 as the inner-jet gases and for inlet radius ratios, r_I/r_O, of 0.50, 0.60, and 0.7. Typical frames used to obtain the apparent containment from these high-speed motion pictures are shown in Fig. 18. For a given inlet configuration, decreasing the inner-jet gas flow rate decreased the radius at which the inner-jet gas entered the chamber until a limiting radius, such as approximately 2 in. for the r_I = 2.5 in. configuration, was reached. Further decreases in the inner-jet flow rate did not reduce the inner-jet gas radius at the inlet but did result, at other axial locations, in a reduction of the inner-jet radius at which the gas become less dense. Single frames from the high-speed motion pictures showing these trends are presented in Fig. 19. The ratio of the outer-stream volumetric flow rate to the inner-jet volumetric flow ratio and the ratio of the weight flow rates are also shown in the figure. For tests with air as the inner-jet gas, these two ratios are approximately equal. For tests with Freon-11, the volumetric flow rate ratios are approximately 4.7 times the weight flow rate ratios. The fraction of the chamber volume filled with the inner-jet gas was also determined for these photographs. Because the volume fraction is equal to the partial pressure fraction, the data are presented as partial pressure fraction to be consistent with previous results.

The apparent coaxial-jet containment data obtained from tests employing the foam inlet with air and Freon-11 as the inner-jet gas are shown in Figs. 20 and 21, respectively. The minimum velocity ratio, V_{BAO}/V_I, was between 8 and 10 for the tests with air as the inner-jet gas. Data could not be obtained from the tests for r_I/r_O = 0.70 and Freon-11 as the inner-jet gas due to nonuniformities or excessive local radial flow within the foam inlet. The maximum inner-jet gas containment volume for all the flow conditions investigated was less than expected and is attributed to the inward radial flow within the foam inlet. For some conditions, the interface between the inner-jet gas and the outer-stream gas was not clearly defined. This was attributed to either mixing in the foam or short circuiting of flow from the outer plenum through the foam onto the inner plenum before entering the chamber. The data symbols which are flagged indicate such dilution or mixing occurred and probably have inner-jet gas concentrations less than indicated by the symbol.

A comparison of the present data obtained employing the foam inlet and the previous data obtained employing the screen inlet (Ref. 4) for $r_I/r_O = 0.5$ is presented in Fig. 22. This comparison shows that the average inner-jet gas containment was not changed for $\bar{P}_I/P > 0.1$. The results from these tests with the foam inlets have shown that, although the nature of the flow was markedly changed, the average inner-jet gas volume within the chamber did not increase in the region of interest.

Containment with a Foam and Porous Plate Inlet

Because of the above results with the foam inlet, the inlet was modified to insure that the inner-jet gas inlet radius would be maintained regardless of inner-jet gas flow rates. This was accomplished by extending the inner-jet gas plenum wall to the inlet plane and replacing the inner-jet foam with a porous plate as shown in Fig. 5c. The apparent inner-jet gas containment for this inlet is shown in Fig. 23 for air and Freon-11 as the inner-jet gases. The flagged symbols indicate flow conditions for which a small amount of recirculation occurred near the exhaust nozzle. As shown by the photographs in Fig. 10d, mixing caused by eddies from the inner-jet gas plenum wall occurred for tests with this inlet. The maximum weight flow ratio for flow without recirculation can probably be increased by use of other porous material and plenum wall length combinations.

The apparent containment with Freon-11 as the inner-jet gas for tests with the foam inlet and the foam and porous plate inlet are compared in Fig. 24 with previous results (Ref. 4) for tests with the screen inlet. The apparent containment volume with the foam and perforated plate inlet for $W_{BAO}/W_I \approx 25$ is a factor of two higher than the data for tests with the other inlets.

Comparison of Results with Requirements

The fluid mechanics performance requirements for open-cycle gaseous nuclear rockets were outlined in Ref. 2. High-, intermediate-, and low-performance regions were defined for a mission which would probably include an orbital nuclear-stage start up and are shown in Fig. 25. The nominal engine design point requires 20 percent of the engine volume to be filled with fuel for a ratio of propellant flow rate to fuel flow rate of 35. The volume fraction was selected from pressure level considerations and the weight flow ratio was chosen from economic considerations so that fuel costs would not be the major mission cost. Increasing either of these parameters at no expense to the other is desirable.

The best data from Ref. 4 for tests with air and Freon-11 as the inner-jet gases lie predominantly in the intermediate-performance region (Fig. 25). The best data from the present tests are in the high-performance region and indicate that the containment characteristics for confined coaxial-flow jets have apparently been improved during this study. However, because of the difficulty of interpreting photographs, actual integration of concentration distributions will be required before firm conclusions can be made.

The cavity flow in the full-scale reactor configuration shown in Fig. 1 is divided into three regions. The studies described in this report are applicable to the central "coaxial-flow region" in Fig. 1 if the flow at the exit of the "developing flow region" can be made similar to that created by the inlets in the present tests. The creation of uniform flow at the exit of this developing flow region is shown to be of great importance by the results of the tests described in the present report.

REFERENCES

1. Weinstein, H. and R. G. Ragsdale: A Coaxial Flow Reactor - A Gaseous Nuclear Rocket Concept. Preprint 1518-60, American Rocket Society, Inc., 1960.

2. Ragsdale, R. G. and F. E. Rom: Gas-Core Reactor Work at NASA/Lewis. NASA Technical Memorandum NASA TM X-52309, 1967.

3. Ragsdale, R. G. and C. D. Lanzo: Some Recent Gaseous Reactor Fluid Mechanics Experiments. NASA Technical Memorandum NASA TM X-52583. Preprint for Fifth Propulsion Joint Specialists Conference, Colorado Springs, Colorado, June 9-13, 1969.

4. Johnson, B. V.: Experimental Study of Multi-Component Coaxial Flow Jets in Short Chambers. United Aircraft Research Laboratories Report G910091-16, April 1968. Also issued as NASA Report CR-1190, October 1968.

5. McLafferty, G. H. and H. E. Bauer: Studies of Specific Nuclear Light Bulb and Open-Cycle Vortex-Stability Gaseous Nuclear Rocket Engines. United Aircraft Research Laboratories Report F-910093-37, prepared under NASA Contract NASw-847, September 1967.

6. Chin, J. H., et al.,: Adiabatic Wall Temperature Downstream of a Single, Tangential Injection Slot. ASME Preprint 58-A-107, 1958.

7. Seban, R. A.: Heat Transfer and Effectiveness for a Turbulent Boundary Layer With Tangential Fluid Injection. ASME Journal of Heat Transfer, pp. 303-312, November 1960.

8. Kacker, S. C. and J. H. Whitelaw: The Effect of Slot Height and Slot-Turbulence Intensity on the Effectiveness of the Uniform Two-Dimensional Wall Jet. ASME Paper No. 68HT-4, 1968.

9. Kendall, J. S., A. E. Mensing, and B. V. Johnson: Containment Experiments in Vortex Tubes with Radial Outflow and Large Superimposed Axial Flow. United Aircraft Research Laboratories Report F-910091-12, 1968. Also issued as NASA CR-993, March 1968.

10. DISA Electronics: Instruction and Service Manual for Type 55D01 Anemometer Unit.

11. Zawacki, T. S. and H. Weinstein: Experimental Investigation of Turbulence In the Mixing Region Between Coaxial Streams. NASA CR-959, February 1968.

REFERENCES (Continued)

12. Leithem, J. H., R. A. Kulik, and H. Weinstein: Turbulence in the Mixing Region Between Ducted Coaxial Streams. NASA CR-1335, July 1969.

13. Kulik, R. A., J. H. Leithem, and H. Weinstein: Effect of Free Stream Turbulence on Coaxial Mixing. NASA CR-1336, May 1969.

14. Michalke, A.: On Spatially Growing Disturbances in an Inviscid Shear Layer. Journal of Fluid Mechanics, Vol. 23, Part 3, pp. 521-544, 1965.

15. Freymuth, P.: On Transition in a Separated Laminar Boundary Layer. Journal of Fluid Mechanics, Vol. 25, Part 4, pp. 683-704, 1966.

16. Clark, J. W., R. C. Stoeffler, and P. G. Vogt: Research on Instabilities in Atmospheric Flow Systems Associated with Clear Air Turbulence. United Aircraft Research Laboratories Report H910563-9, prepared under NASA Contract NASw-1582, June 1969.

LIST OF SYMBOLS

D_N	Diameter of exhaust nozzle, in. or ft
f	Frequency, cycles per sec
f^*	Frequency of wave determined from motion picture frames, $N/\Delta N$, cycles per sec
L	Length in chamber, in. or ft
L_C	Length of chamber from inlet plane to beginning of nozzle, in. or ft
L_N	Length of chamber from inlet plane to nozzle throat, in. or ft
N	Number of motion picture frames per second
ΔN	Number of motion picture frames between waves or turbles
P	Total pressure, lb/ft^2 or atm
P_I	Local partial pressure of inner-jet gas, lb/ft^2
$\bar{P}_I$	Average partial pressure of inner-jet gas, lb/ft^2
Q_I	Inner-jet gas volume flow rate, ft^3/sec
Q_O	Outer-stream volume flow rate, ft^3/sec
r	Local radius from center of chamber, in. or ft
r_B	Buffer-stream radius at inlet, in. or ft
r_C	Radius of centerbody, in. or ft
r_I	Inner-jet radius at inlet, in. or ft
r_O	Peripheral-wall radius, in. or ft
r^*	Outermost radius of dense inner-jet gas, in. or ft
v'	Rms value of fluctuating component of local velocity, ft/sec

LIST OF SYMBOLS (Continued)

V	Local velocity, ft/sec
V^*	Velocity for normalizing shear layer profile, maximum value of outer stream measured 1 in. downstream of inlet plane, ft/sec
V_B	Inlet velocity of buffer stream, ft/sec
V_{BAO}	Average inlet velocity of combined outer stream and buffer stream, $W_{BAO}/\rho_{BAO}\pi(r_O^2 - r_I^2)$, ft/sec
V_I	Inlet velocity of inner jet, ft/sec
V_O	Inlet velocity of outer stream, ft/sec
W_{BAO}	Combined weight flow rate of outer-stream and buffer-stream gases, lb/sec
W_F	Weight flow rate of fuel or simulated fuel, lb/sec
W_I	Weight flow rate of inner-jet gas, lb/sec
W_O	Weight flow rate of outer-stream gas, lb/sec
W_P	Weight flow rate of propellant or simulated propellant, lb/sec
y	Distance perpendicular to mean flow direction, in. or ft
Z	Axial distance downstream from inlet plane, in. or ft
β_r	Nondimensional cyclic frequency, $2\pi fL/V^*$
ϕ	Azimuthal location, deg
θ	Momentum thickness of shear layer, $\int_{-\infty}^{\infty}\left(\frac{V - V_{min}}{V_{max} - V_{min}}\right)\left(\frac{V_{max} - V}{V_{max} - V_{min}}\right) dy$

SKETCH OF COAXIAL-FLOW GASEOUS-CORE NUCLEAR ROCKET ENGINE SHOWING FLUID MECHANICS ASPECTS

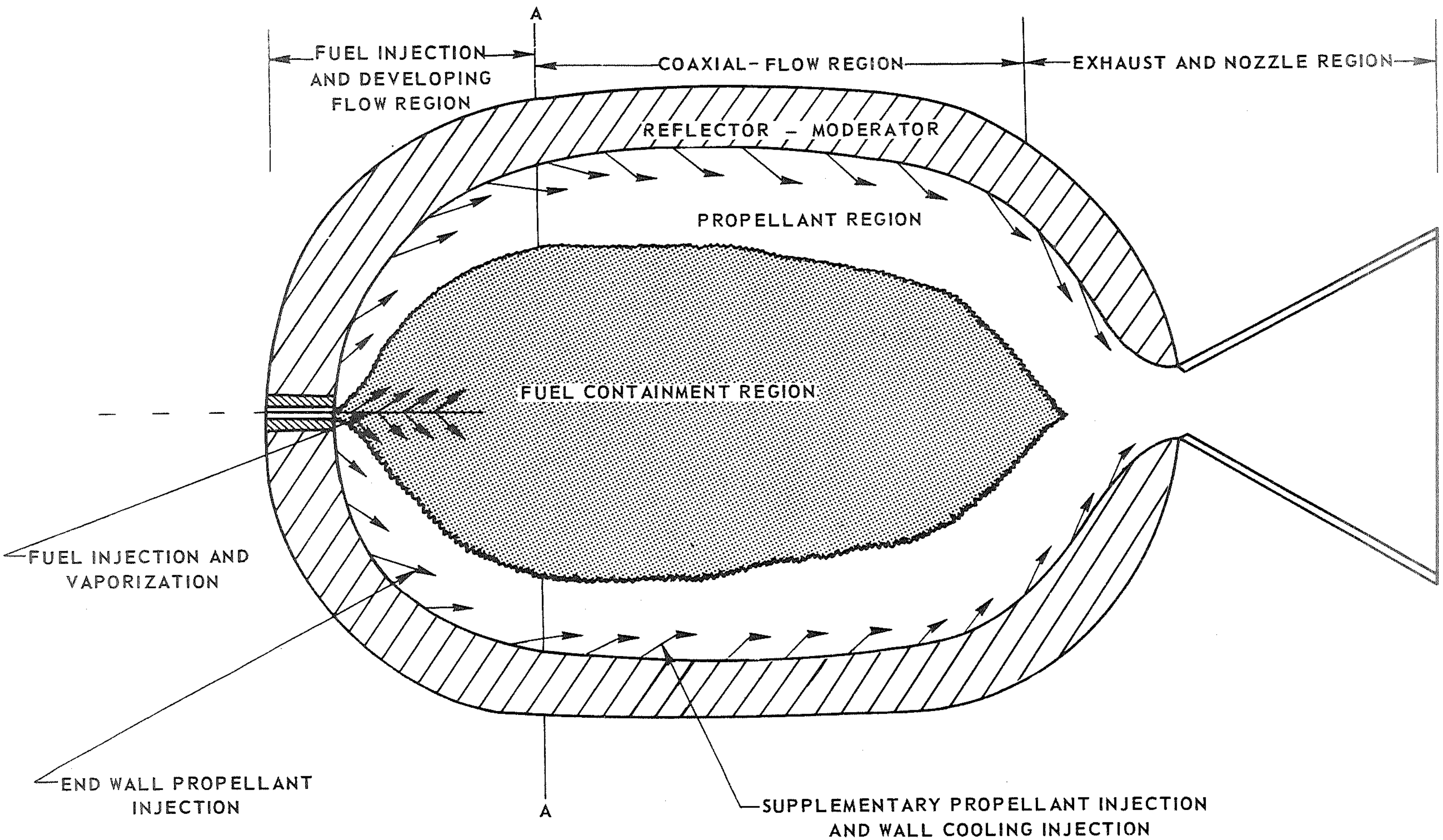

FIG. 1

SCHEMATIC OF TEST APPARATUS

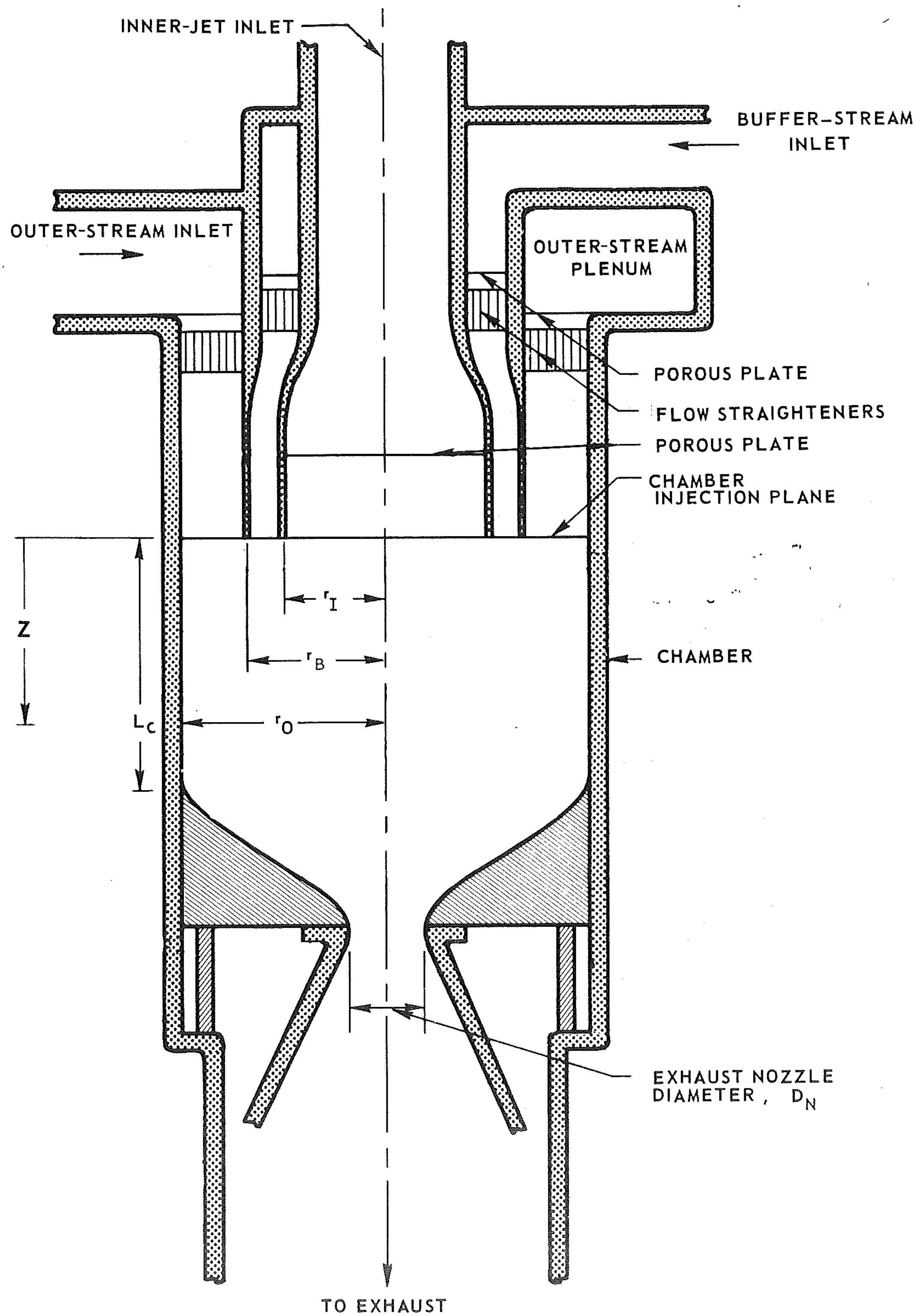

PHOTOGRAPH OF TEST FACILITY SHOWING FLOW SYSTEM

NOZZLE FOR MEASURING BUFFER-STREAM AND OUTER-STREAM AIR FLOW RATE

AND HEAT EXCHANGERS NOT SHOWN IN PHOTOGRAPH

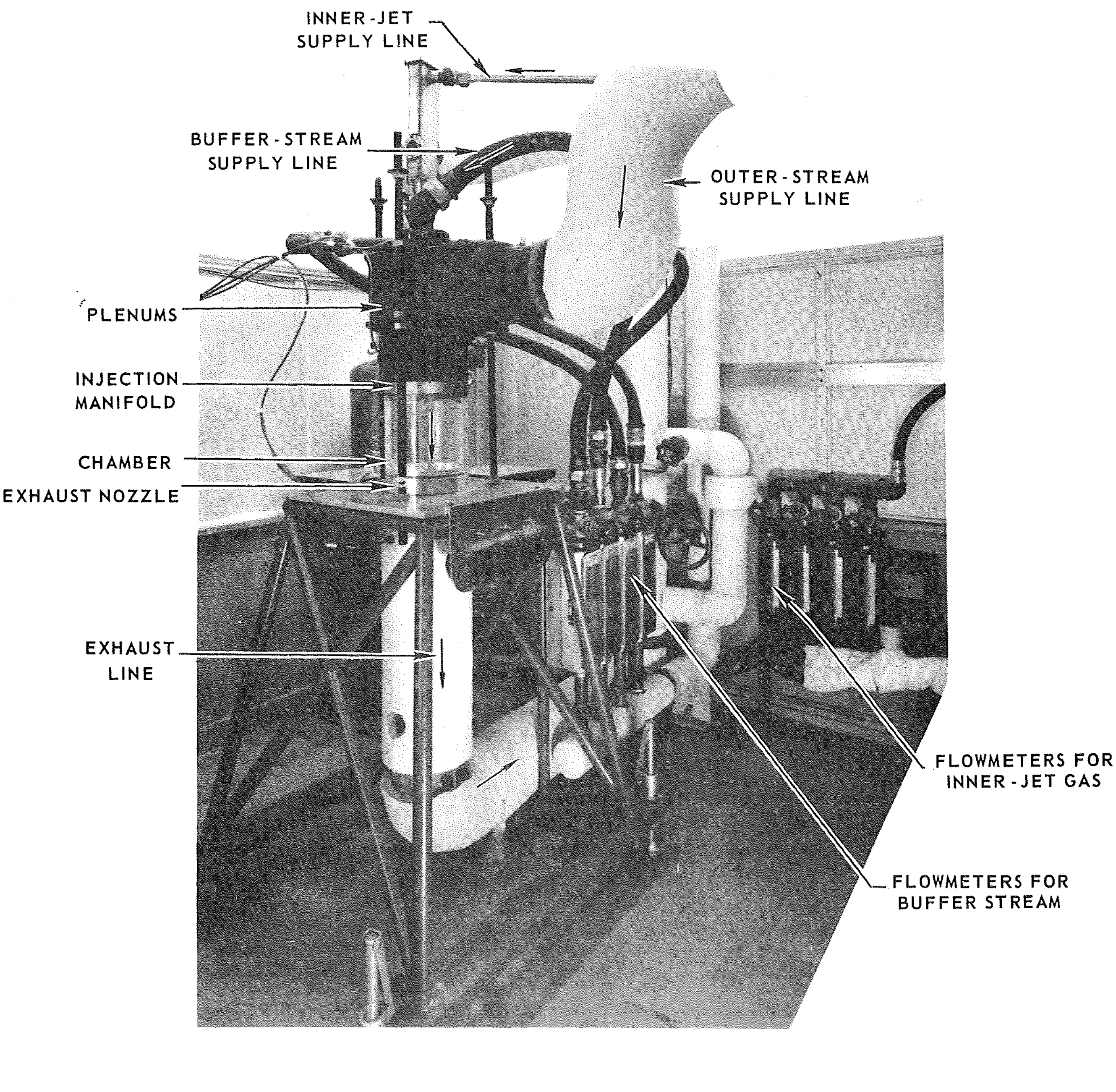

SKETCHES OF CHAMBER CONFIGURATIONS

CHAMBER INSIDE DIA FOR ALL CONFIGURATIONS – 10 IN.

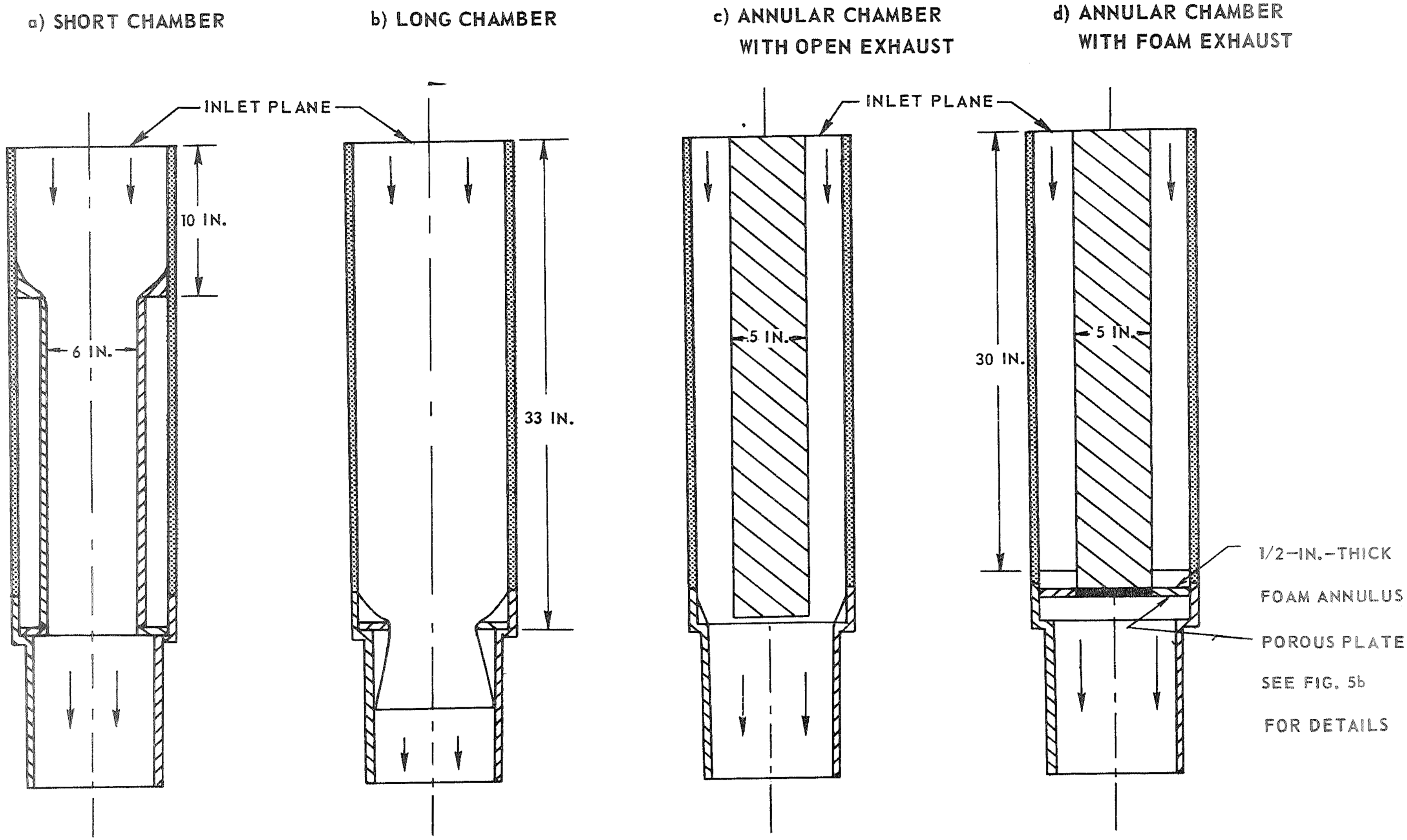

FIG. 4

SKETCHES OF INLET CONFIGURATIONS

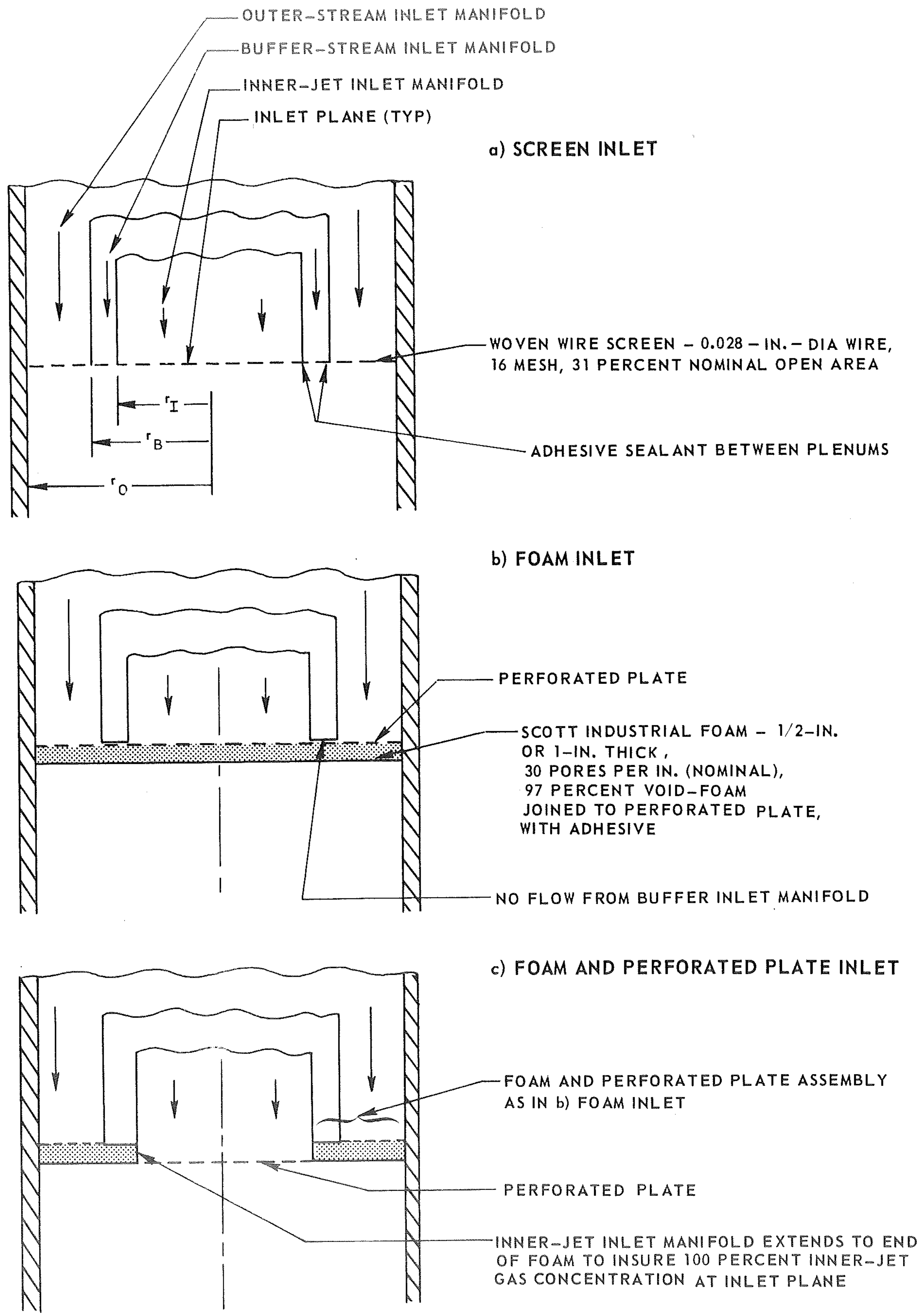

CONTINUED

SKETCHES OF INLET CONFIGURATIONS

d) ANNULAR FOAM INLET

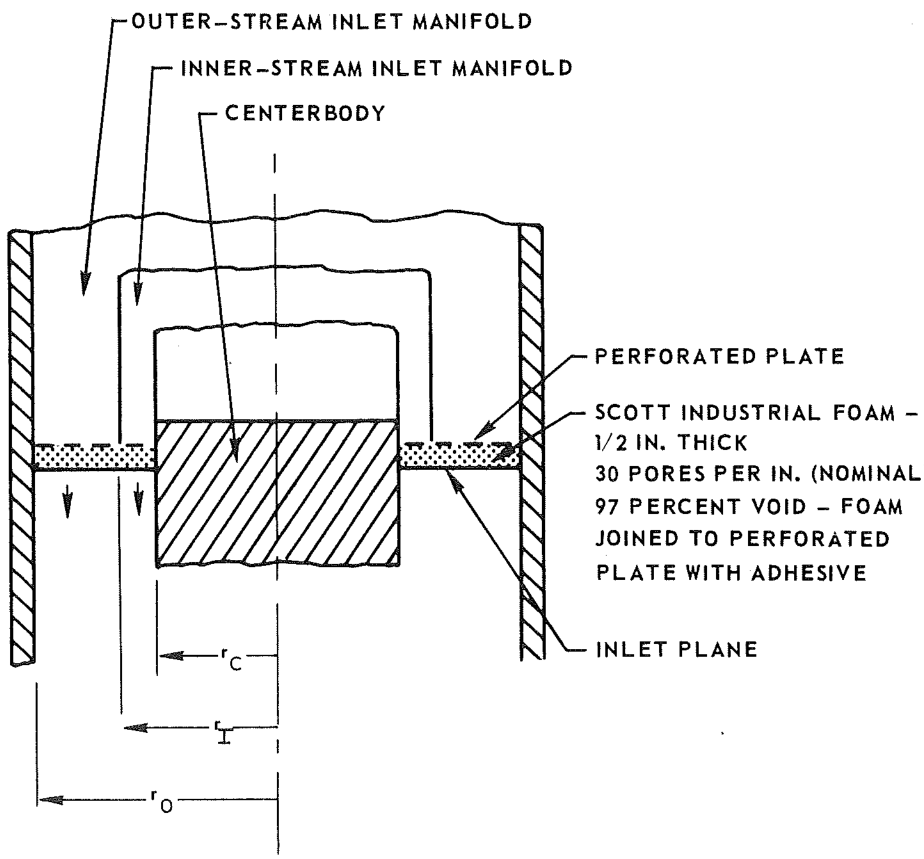

SCHEMATIC OF OPTICAL SYSTEM FOR FLOW VISUALIZATION PHOTOGRAPHY

TOP VIEW

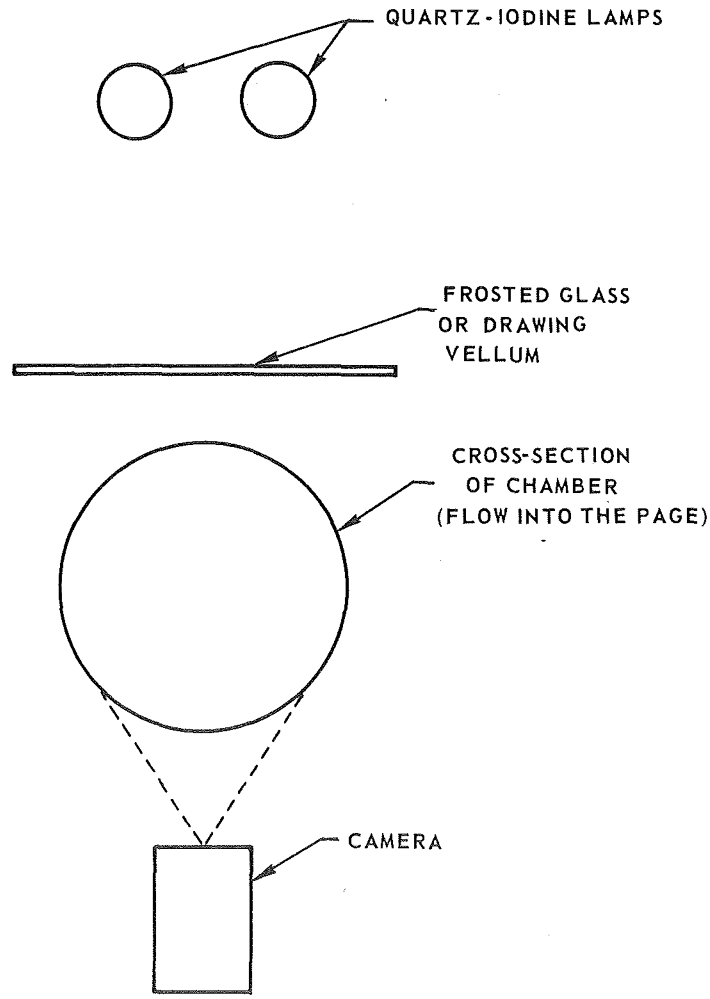

HOT-WIRE AND FLOW VISUALIZATION RESULTS WITH APPROXIMATELY EQUAL VELOCITIES AND WITH SCREEN INLET

CASE 9067

t = 0.00 SEC

t = 0.012 SEC

t = 0.024 SEC

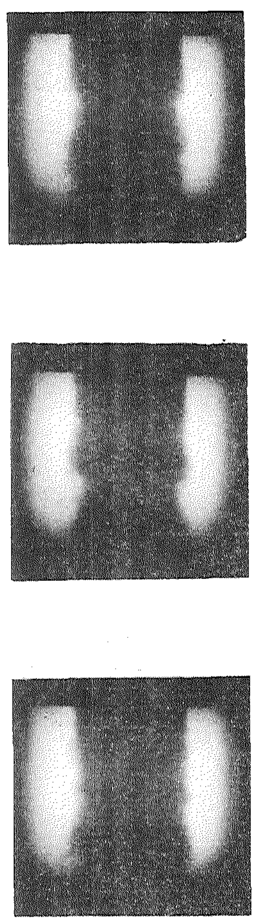

CONFIGURATION – SHORT CHAMBER AND SCREEN INLET WITH

$r_I/r_O = 0.50$ AND $r_B/r_O = 0.65$

FLOW CONDITION – $V_O \approx V_B \approx 20$ FT/SEC, $V_I \approx 18$ FT/SEC, GAS-AIR

WAVE DISTURBANCE DATA OBTAINED FROM HIGH-SPEED MOTION PICTURE FRAMES

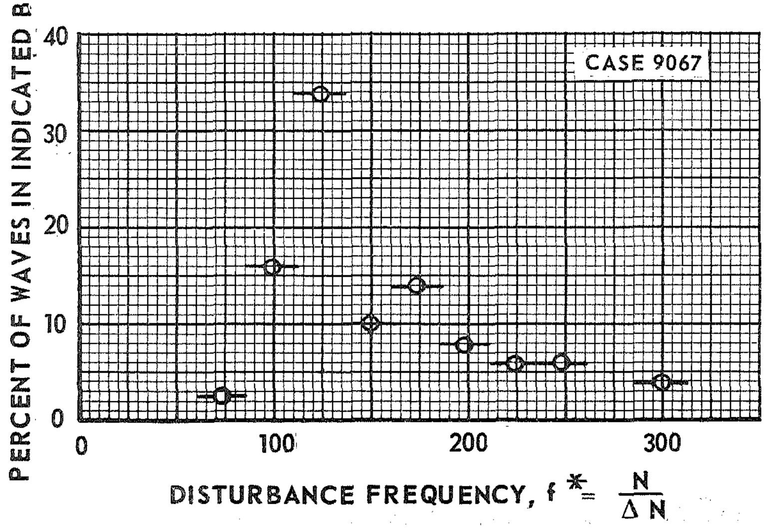

HOT WIRE SPECTRAL DATA OBTAINED AT RADIUS, r = 2.5 IN.

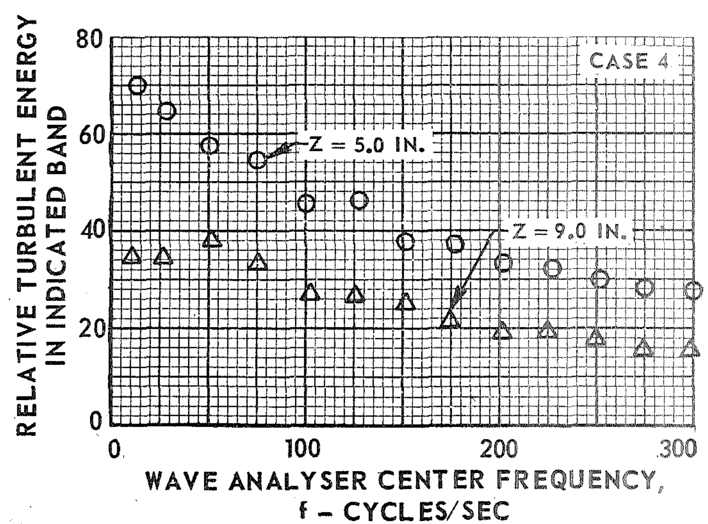

FIG. 7

HOT-WIRE AND FLOW VISUALIZATION RESULTS AT LOW VELOCITY RATIOS WITH SCREEN INLET

CONFIGURATION – SHORT CHAMBER AND SCREEN INLET WITH $r_I/r_O = 0.05$ AND $r_B/r_O = 0.65$

FLOW CONDITION – $V_O \approx V_B \approx 40$ FT/SEC, $V_I \approx 20$ FT/SEC, GAS–AIR

CASE 9069

t = 0.00 SEC

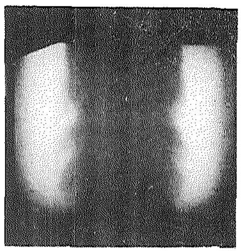

t = 0.005 SEC

t = 0.010 SEC

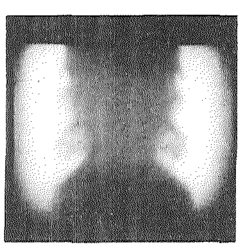

WAVE DISTURBANCE DATA OBTAINED FROM HIGH–SPEED MOTION PICTURE FRAMES

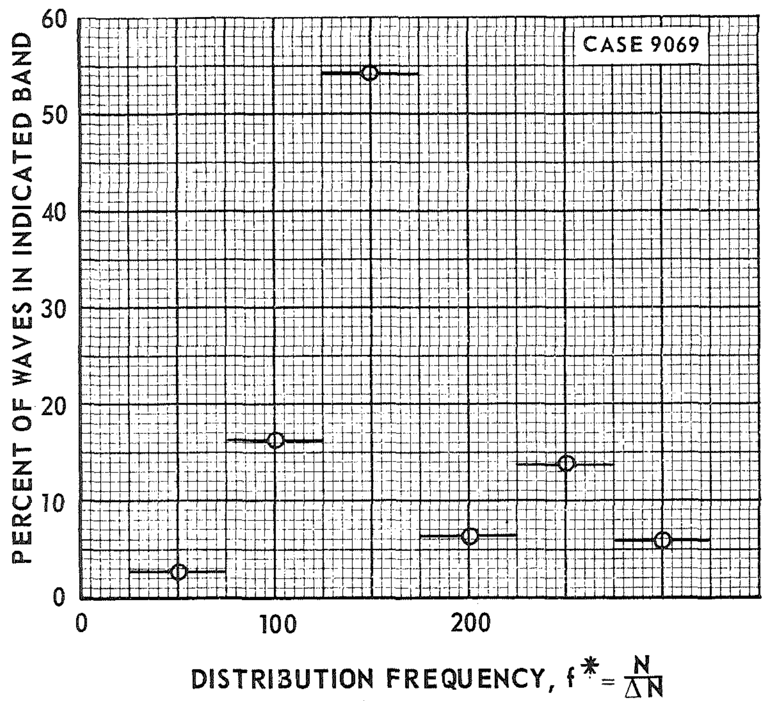

HOT-WIRE SPECTRAL DATA OBTAINED AT RADIUS, r = 2.5 IN.

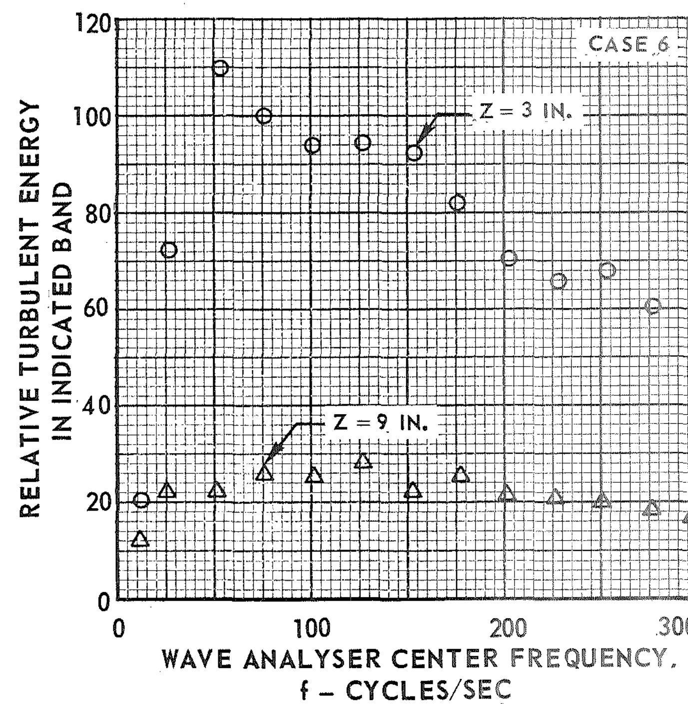

FIG. 8

TURBULENT INTENSITY DISTRIBUTION FOR SCREEN AND FOAM INLETS

CONFIGURATION – CHAMBER WITH $r_I/r_O = 0.50$ AND $r_B/r_O = 0.65$

FLOW CONDITION $V_O \approx V_B \approx 40$ FT/SEC, $V_I \approx 20$ FT/SEC, GAS–AIR

TURBULENT INTENSITY OBTAINED WITH HOTWIRE ANEMOMETER

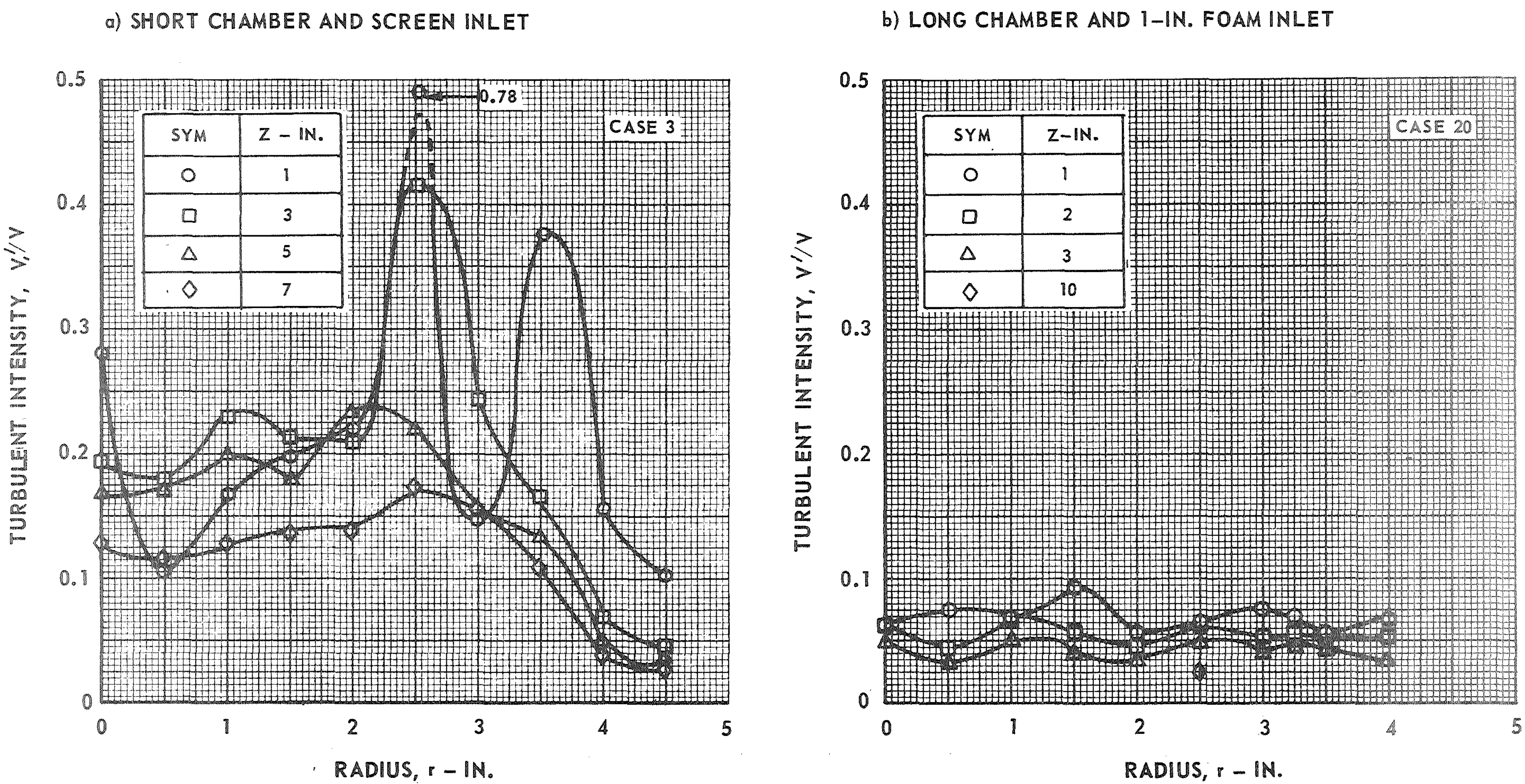

FIG. 9

EFFECT OF INLET FLOW CONDITIONS ON WAVE DISTURBANCE CHARACTERISTICS FOR COAXIAL JETS

CONFIGURATION – SHORT CHAMBER

FLOW CONDITION – $V_{BAO} \approx 80$ FT/SEC, OUTER, BUFFER AND INNER JET GASES – AIR, AIR AND FREON II

a) CASE 9013 (REF. 4)

SCREEN INLET

$r_I/r_O = 0.50$

$V_{BAO}/V_I = 18.9$

$V_B/V_{BAO} = 0.89$

$W_{BAO}/W_I = 10.2$

b) CASE 9014 (REF. 4)

SCREEN INLET

$r_I/r_O = 0.50$

$V_{BAO}/V_I = 20.1$

$V_B/V_{BAO} = 0.45$

$W_{BAO}/W_I = 11.4$

c) CASE 79

FOAM INLET

$r_I/r_O = 0.50$

$V_{BAO}/V_I = 28.8$

$W_{BAO}/W_I = 20.2$

d) CASE 124

FOAM AND PERFORATED PLATE INLET

$r_I/r_O = 0.60$

$V_{BAO}/V_I = 45.8$

$W_{BAO}/W_I = 18.8$

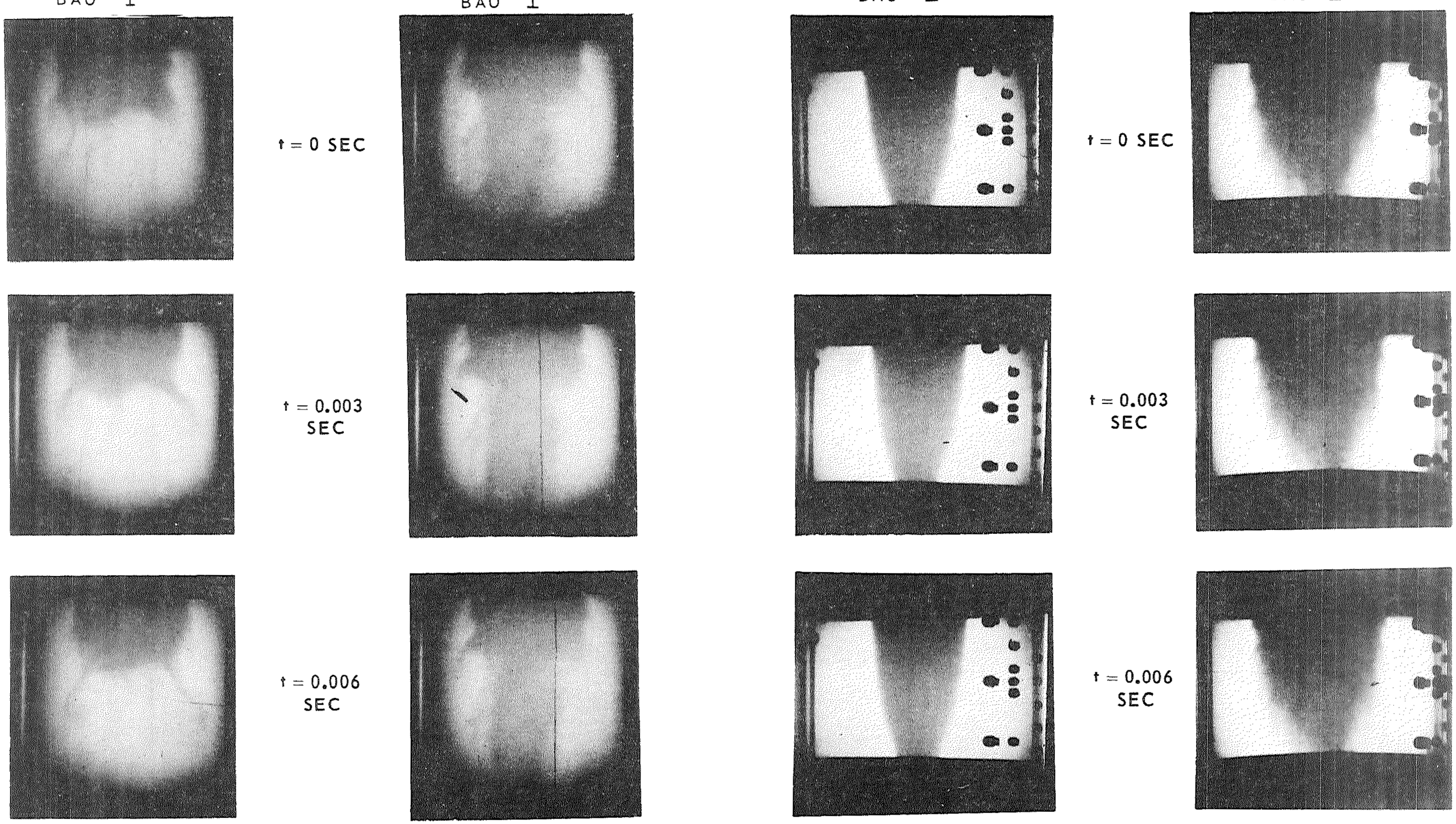

FIG. 10

H-910091-21

WAVE DISTURBANCE SPECTRUM FOR AIR AND FREON-II AS INNER JET GASES

DATA OBTAINED FROM HIGH SPEED MOTION PICTURES

CONFIGURATION – SHORT CHAMBER AND 1/2 IN. FOAM INLET WITH $r_I/r_O = 0.5$ AND $r_B/r_O = 0.65$

FLOW CONDITION – OUTER STREAM GAS-AIR, $V_{BAO} \approx 80$ FT/SEC, $V_B = 0$ FT/SEC

θ OBTAINED FOR CASE 75 (SEE FIG. 14)

$V^* \approx 94$ FT/SEC,

SYMBOL	□	△	○	◇	▽
W_{BAO}/W_I	∞ TO 200	200 – 100	100 – 50	50 – 20	20 – 10

a) INNER-JET GAS-AIR

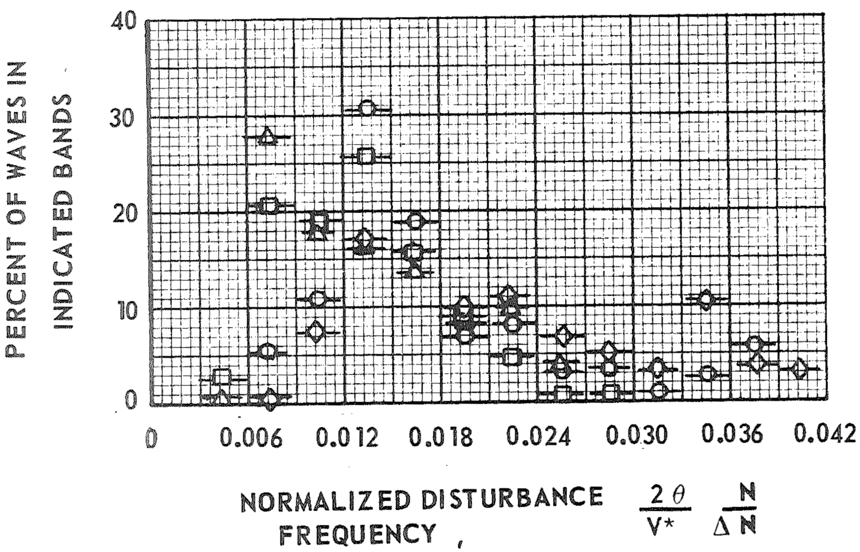

b) INNER-JET GAS-FREON-II

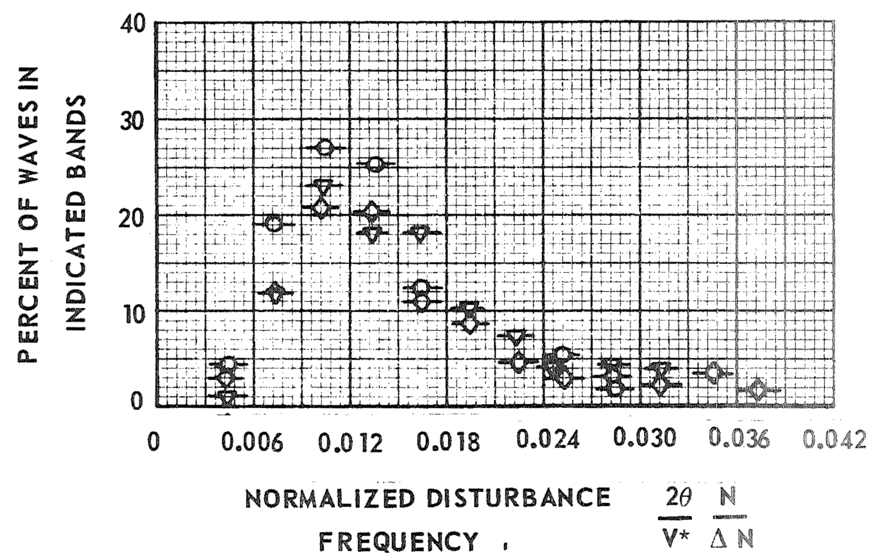

FIG. 11

COMPARISON OF 2-D INVISCID THEORETICAL GROWTH RATE AND COAXIAL-JET EXPERIMENTAL WAVE DISTURBANCE SPECTRUM

a) THEORETICAL GROWTH FACTOR

RESULT FOR CONSTANT - DENSITY FLUID AND VELOCITY PROFILE $V = (V_0/2)[1 + \tanh(y/L)]$

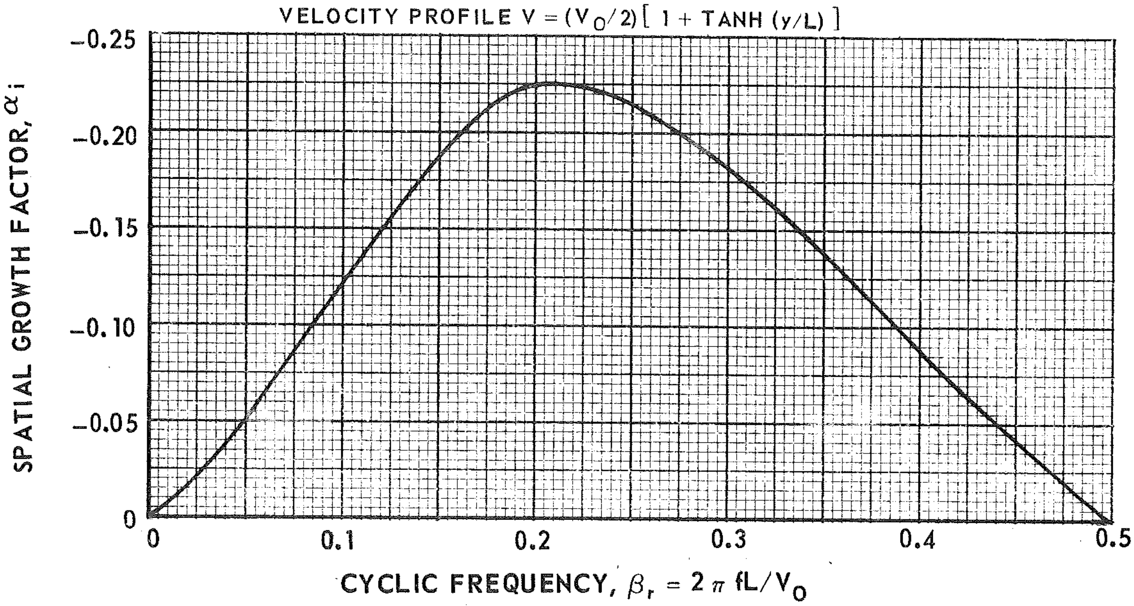

b) EXPERIMENTAL DISTURBANCE SPECTRUM

RESULTS FROM FIG. 11a AND 11b ARE AVERAGE VALUES FOR EACH DISTURBANCE FREQUENCY BAND

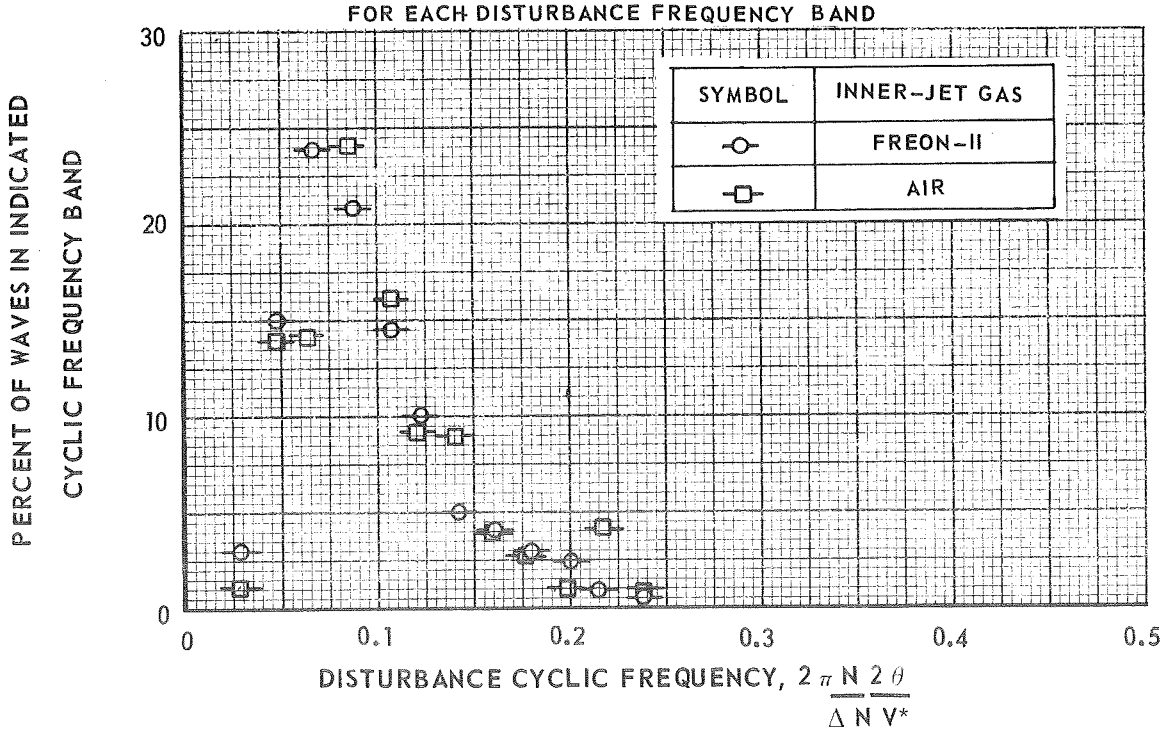

COMPARISON OF VELOCITY PROFILES OBTAINED WITH HOT-WIRE AND PITOT PROBES

CONFIGURATION – SHORT CHAMBER AND 1/2 – IN. FOAM INLET WITH

$r_I / r_O = 0.50$ AND $r_B / r_O = 0.65$

FLOW CONDITION – $V_O = 93.6$, $V_B = V_I = 0$ GAS–AIR

PROFILES MEASURED 1 IN. DOWNSTREAM FROM FOAM

SYMBOL	MEASUREMENT TECHNIQUE	AZIMUTHAL LOCATION, ϕ – DEG
△	HOT–WIRE VELOCITY MEASUREMENTS	0
○	PITOT PRESSURE VELOCITY MEASUREMENTS	15

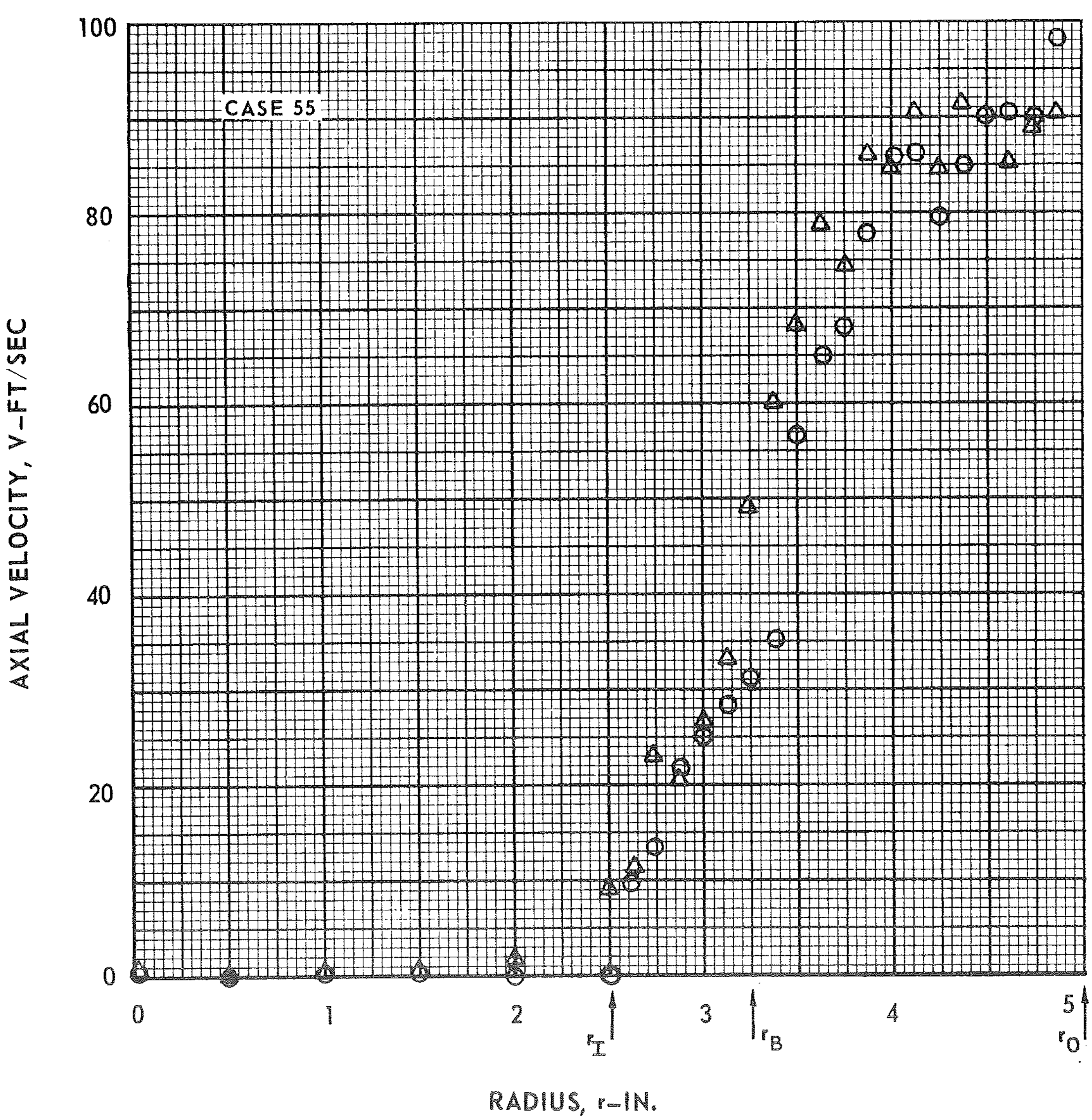

VELOCITY PROFILES NEAR INLET FOR SEVERAL INNER-JET VELOCITIES AT HIGH OUTER-STREAM VELOCITIES

CONFIGURATION – SHORT CHAMBER AND 1/2– IN. FOAM INLET WITH $r_I/r_O = 0.50$ AND $r_B/r_O = 0.65$

PROFILES MEASURED 1 IN. DOWNSTREAM FROM FOAM

SYMBOL	CASE	V_I, FT/SEC	V_B, FT/SEC	V_O, FT/SEC	V_{BAO}, FT/SEC	V_{BAO}/V_I	W_{BAO}/W_I
◇	55	0	0	94	72	∞	∞
△	66	1.8	0	107	83	46	137.2
□	75	2.9	0	105	80	27	81.026
○	67	8.8	0	107	83	9.3	27.98

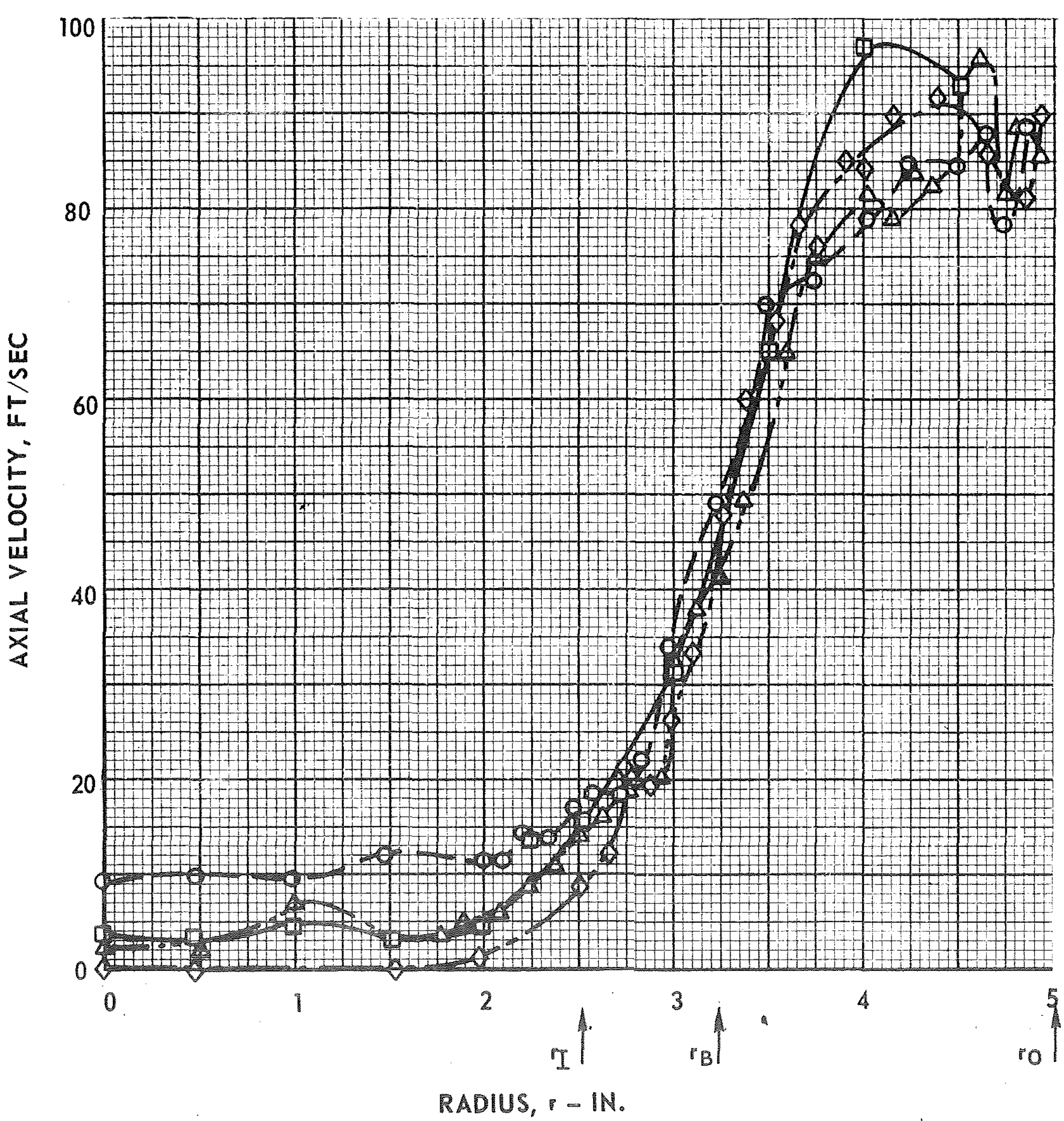

FIG. 15

VELOCITY PROFILES NEAR INLET FOR SEVERAL INNER-JET VELOCITIES AT LOW OUTER-STREAM VELOCITIES

CONFIGURATION – SHORT CHAMBER AND FOAM INLET WITH $r_I/r_O = 0.50$ AND $r_B/r_O = 0.65$

PROFILES MEASURED 1 IN. DOWNSTREAM FROM FOAM

SYMBOL	CASE	V_I, FT/SEC	V_B, FT/SEC	V_O, FT/SEC	V_{BAO}, FT/SEC	V_{BAO}/V_I	W_{BAO}/W_I
□	61	12	0	45	35	3	8.78
△	60	4.6	0	44	34	7	21.28
○	59	1.9	0	44	34	18	51.36
◊	63	0	0	44	34	0	∞

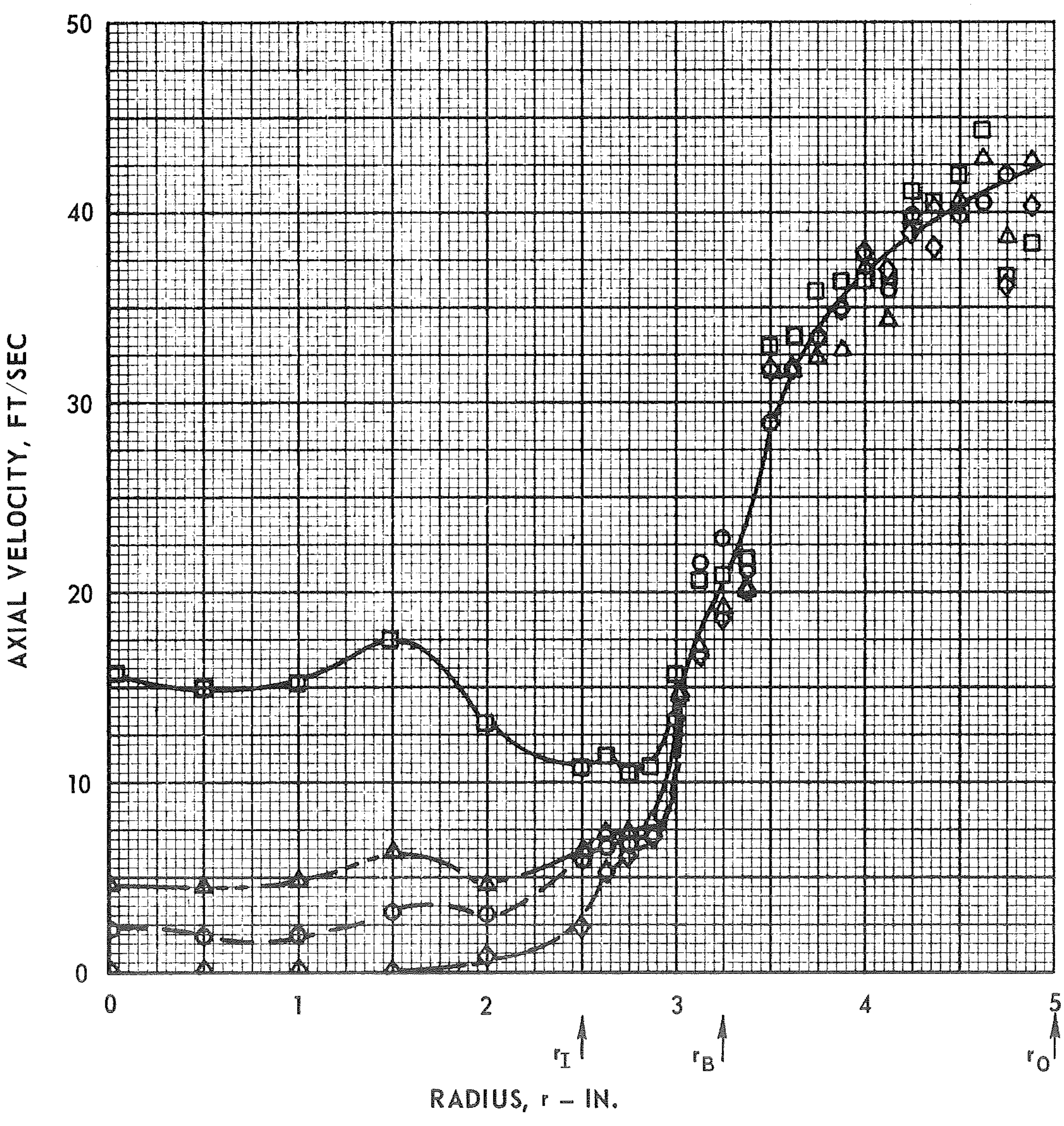

VELOCITY PROFILES AT SEVERAL AXIAL LOCATIONS FOR $V_{BAO}/V_I = 27$

CONFIGURATION – SHORT CHAMBER AND 1/2—IN. FOAM INLET
WITH $r_I/r_O = 0.50$ AND $r_B/r_O = 0.65$

FLOW CONDITION – $V_I = 2.9$ FT/SEC, $V_B = 0$, $V_O \approx 105$ FT/SEC,
$V_{BAO} \approx 80$ FT/SEC $W_{BAO}/W_I = 81$, GAS–AIR

SYMBOL	AXIAL LOCATION DOWNSTREAM FROM FOAM
○	1.0 IN.
□	3.5 IN.
△	6.0 IN.

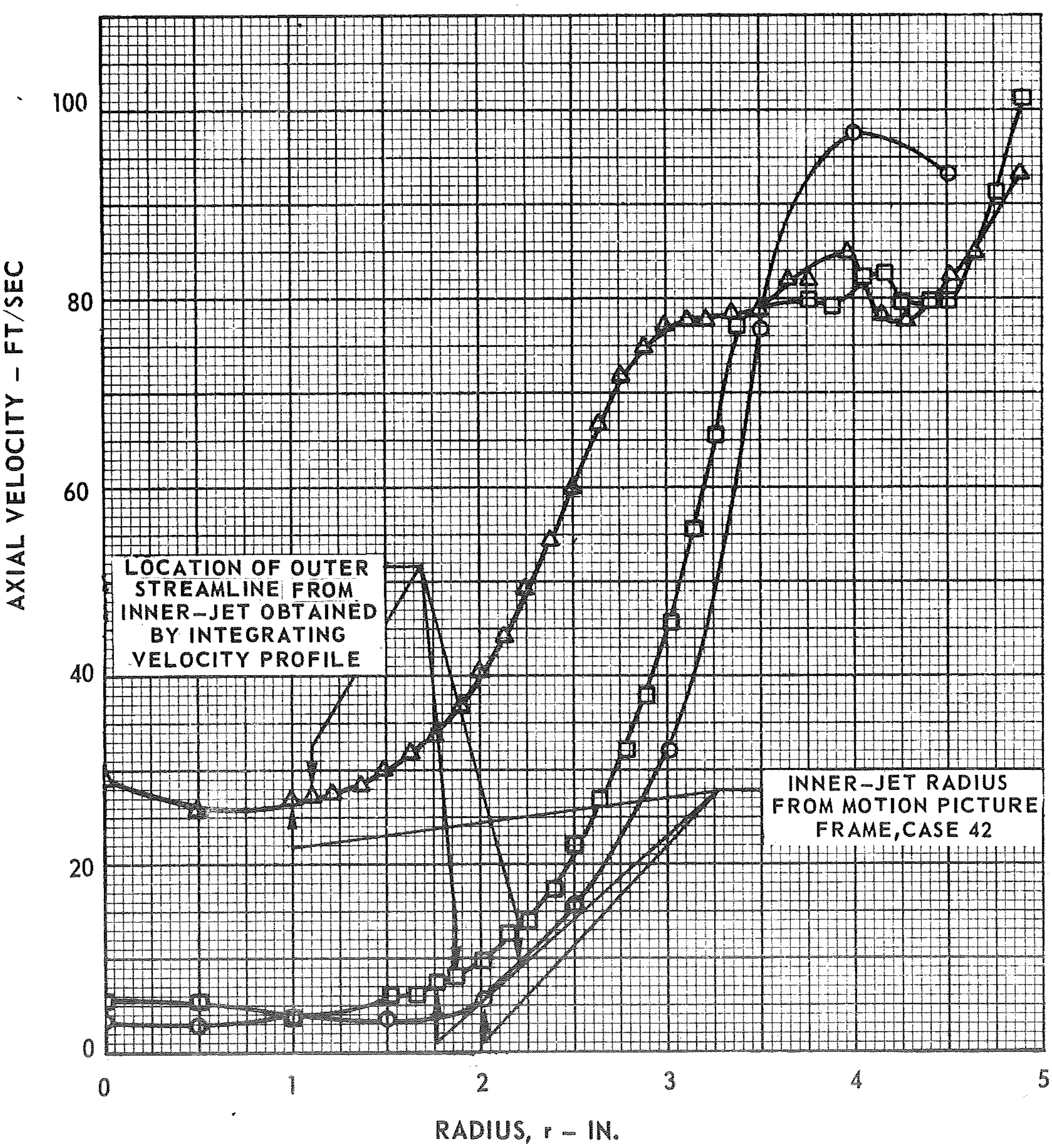

EFFECT OF CONFIGURATION ON WAVE DISTURBANCE CHARACTERISTICS IN LONG CHAMBERS WITH APPROXIMATELY EQUAL VELOCITIES

CONFIGURATION – 1/2-IN. FOAM INLET

FLOW CONDITIONS – $V_O \approx V_B \approx 20$ FT/SEC, GAS-AIR

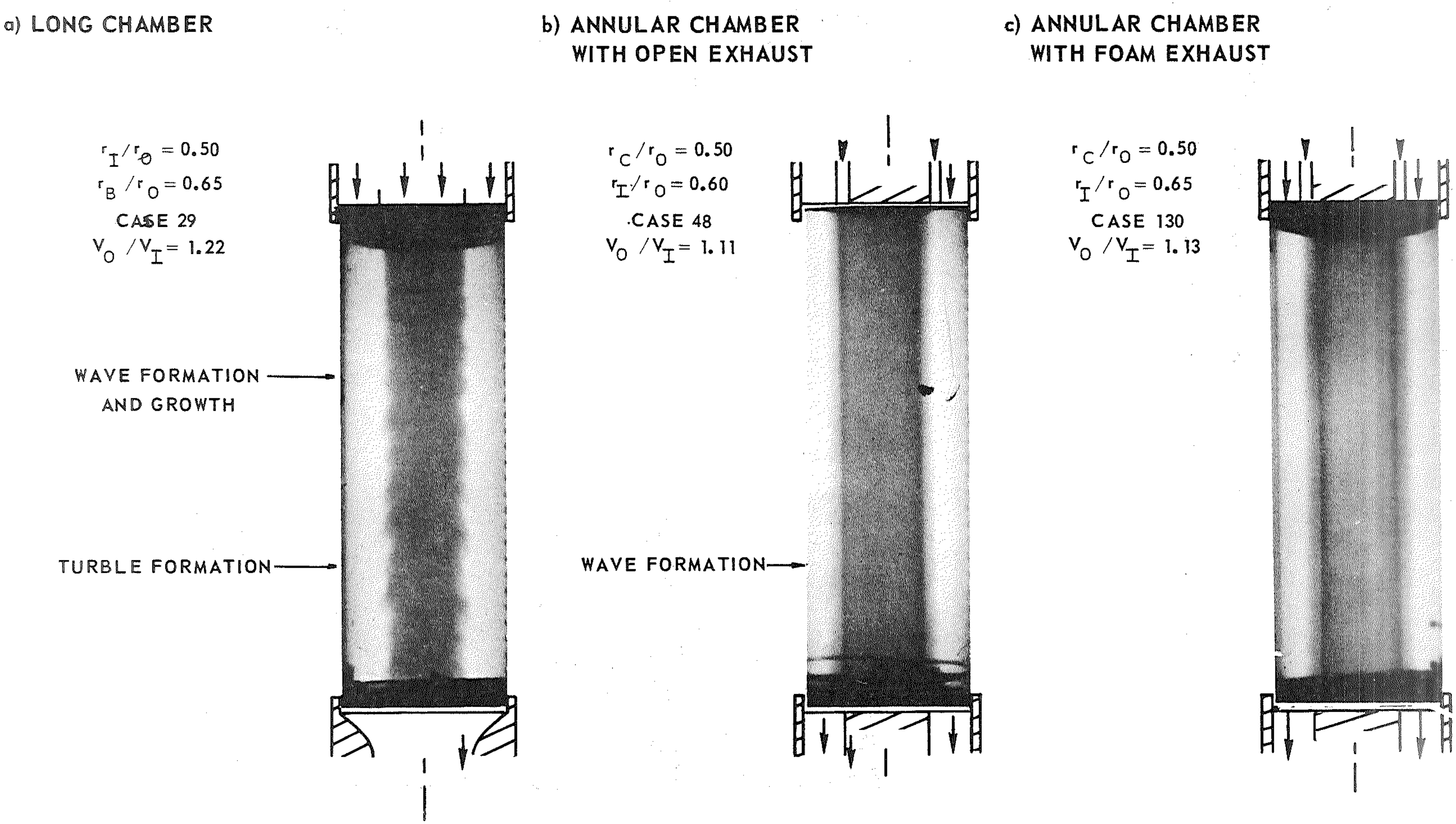

FIG. 17

TYPICAL FRAMES OF HIGH-SPEED MOTION PICTURES USED TO OBTAIN APPARENT COAXIAL-JET CONTAINMENT

CONFIGURATION – SHORT CHAMBER AND 1/2 – IN. FOAM INLET

FLOW CONDITION – $V_{BAO} \approx 80$ FT/SEC, $V_B = 0$, OUTER-STREAM GAS-AIR

INNER-JET GAS-AIR | **INNER-JET GAS-FREON-II**

a) CASE 39
V_I = 10.5 FT/SEC

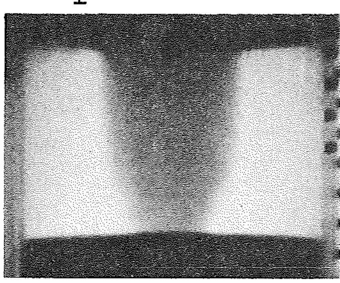

$r_I/r_O = 0.50$
$r_B/r_O = 0.65$

d) CASE 79
V_I = 2.7 FT/SEC

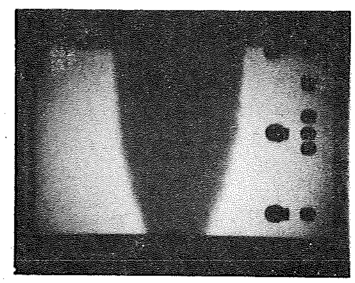

b) CASE 105
V_I = 6.4 FT/SEC

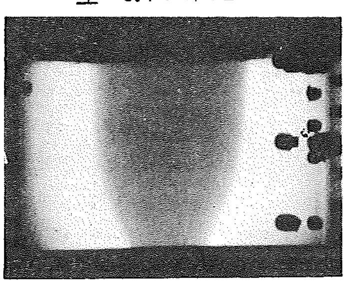

$r_I/r_O = 0.60$
$r_B/r_O = 0.70$

e) CASE 109
V_I = 4.6 FT/SEC

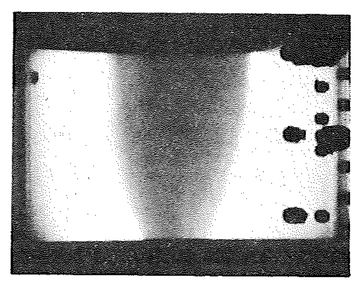

c) CASE 113
V_I = 9.0 FT/SEC

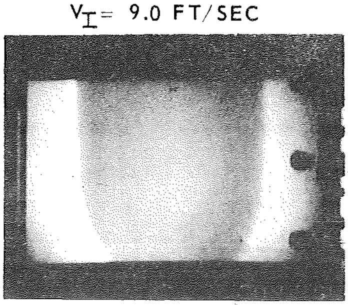

$r_I/r_O = 0.70$
$r_B/r_O = 0.80$

EFFECT OF FLOW RATE RATIO ON INNER-JET GAS CONTAINMENT VOLUME FOR FOAM INLET

CONFIGURATION – SHORT CHAMBER AND 1/2-IN. FOAM INLET WITH $r_I/r_O = 0.50$ AND $r_B/r_O = 0.65$

FLOW CONDITION – $V_{BAO} \approx 80$ FT/SEC, $V_B = 0$, OUTER-STREAM GAS-AIR

INNER-JET GAS-AIR

CASE 39

$W_O/W_I = 24$

$Q_O/Q_I = 24$

$\bar{P}_I/P \approx 0.15$

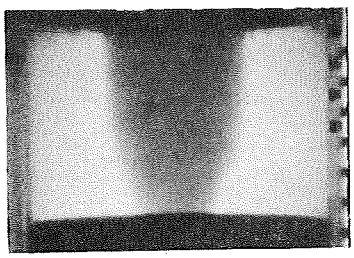

CASE 41

$W_O/W_I = 47$

$Q_O/Q_I = 46$

$\bar{P}_I/P \approx 0.13$

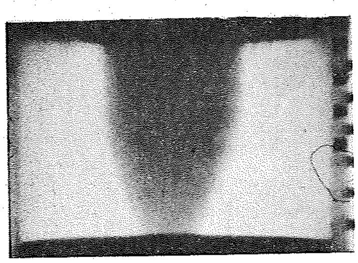

CASE 42

$W_O/W_I = 84$

$Q_O/Q_I = 80$

$\bar{P}_I/P \approx 0.10$

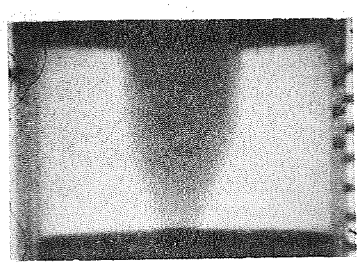

CASE 70

$W_O/W_I = 187$

$Q_O/Q_I = 180$

$\bar{P}_I/P \approx 0.098$

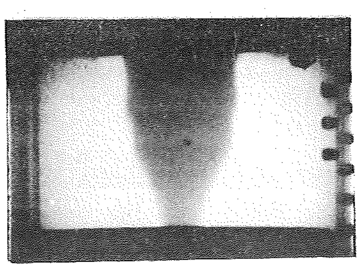

INNER-JET GAS-FREON-11

CASE 79

$W_O/W_I = 20$

$Q_O/Q_I = 86$

$\bar{P}_I/P \approx 0.12$

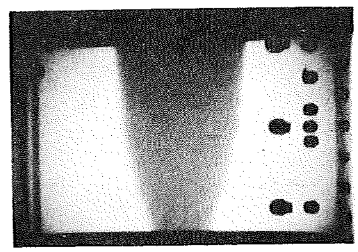

CASE 78

$W_O/W_I = 33$

$Q_O/Q_I = 148$

$\bar{P}_I/P \approx 0.09$

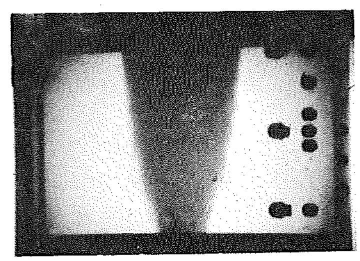

CASE 77

$W_O/W_I = 49$

$Q_O/Q_I = 222$

$\bar{P}_I/P \approx 0.088$

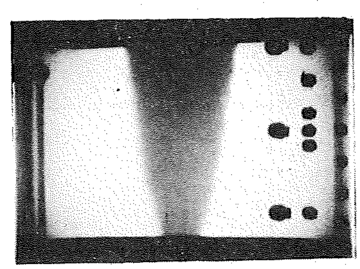

CASE 76

$W_O/W_I = 87$

$Q_O/Q_I = 260$

$\bar{P}_I/P \approx 0.086$

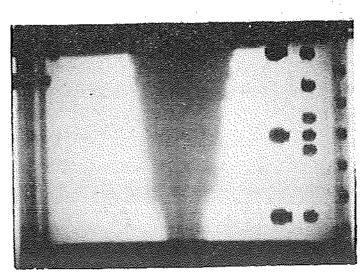

APPARENT COAXIAL-JET CONTAINMENT WITH FOAM INLET AND AIR AS INNER-JET GAS

CONFIGURATION – SHORT CHAMBER WITH 1/2-IN. FOAM INLET

FLOW CONDITIONS – $V_{BAO} \approx 80$ FT/SEC, $V_I = 0$, GAS–AIR

FLAGGED SYMBOL INDICATES INNER-JET GAS WAS PROBABLY DILUTED DUE TO MIXING OR OUTER GAS RADIAL FLOW IN FOAM

SYMBOL	r_I/r_O	r_B/r_O
□——□	0.70	0.80
△– – –△	0.60	0.73
○- - -○	0.50	0.65

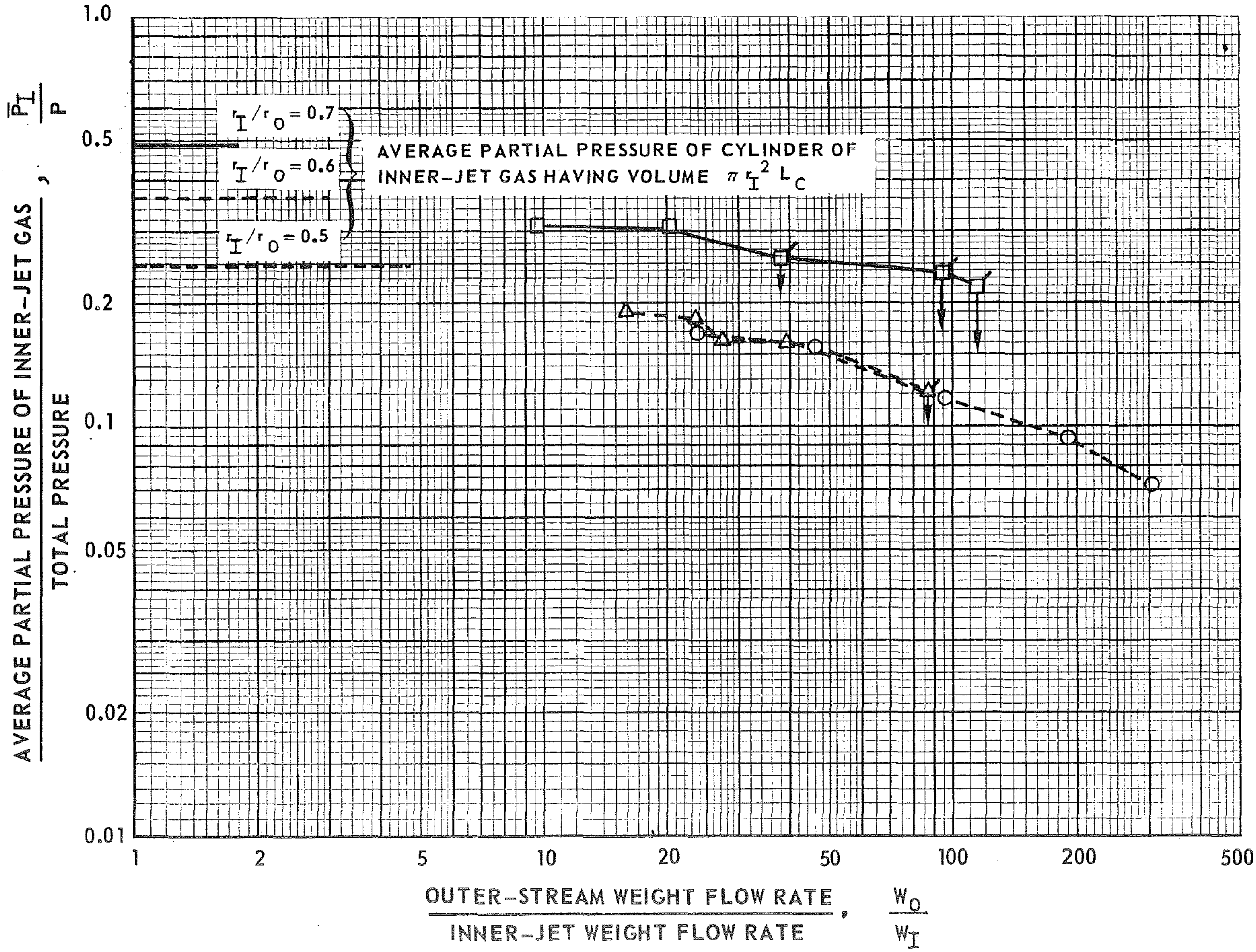

APPARENT COAXIAL-JET CONTAINMENT WITH FOAM INLET AND FREON-11 AS INNER-JET GAS

CONFIGURATION – SHORT CHAMBER AND 1/2-IN. FOAM INLET

FLOW CONDITIONS – $V_{BAO} \approx 80$ FT/SEC, $V_B = 0$, OUTER-STREAM GAS-AIR

FLAGGED SYMBOL INDICATES DILUTION OF INNER-JET GAS DUE TO RECIRCULATION OR RADIAL FLOW AT FOAM INLET

SYMBOL	r_I/r_O	r_B/r_O
▲- - -▲	0.60	0.73
●- - -●	0.50	0.65

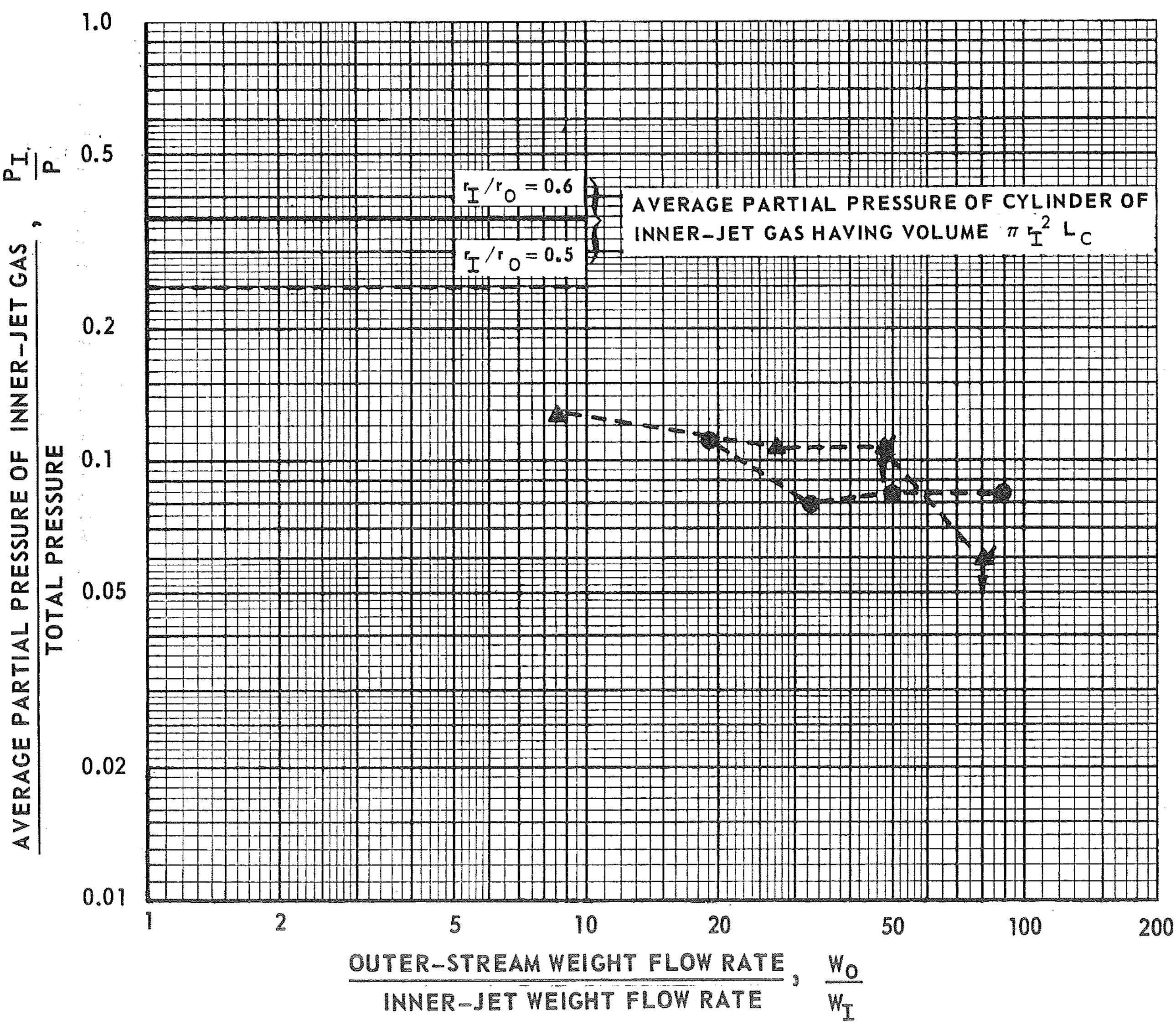

COMPARISON OF APPARENT COAXIAL-JET CONTAINMENT WITH PREVIOUS CONCENTRATION MEASUREMENTS FOR $r_I/r_O = 0.5$

CONFIGURATION – SHORT CHAMBER WITH $r_I/r_O = 0.50$, $r_B/r_O = 0.65$

FLOW CONDITION – $V_{BAO} \approx 80$ FT/SEC, BUFFER AND OUTER STREAM GAS-AIR

SYMBOL	INLET CONFIGURATION	INNER-JET GAS	ρ_I/ρ_{BAO}	DATA OBTAINED
△– – –△	SCREEN	AIR	1.0	REF. 6
▲– – –▲	1/2-IN. FOAM	AIR	1.0	PHOTOGRAPHS
○——○	SCREEN	FREON-11	4.7	REF. 6
●——●	1/2-IN. FOAM	FREON-11	4.7	PHOTOGRAPHS

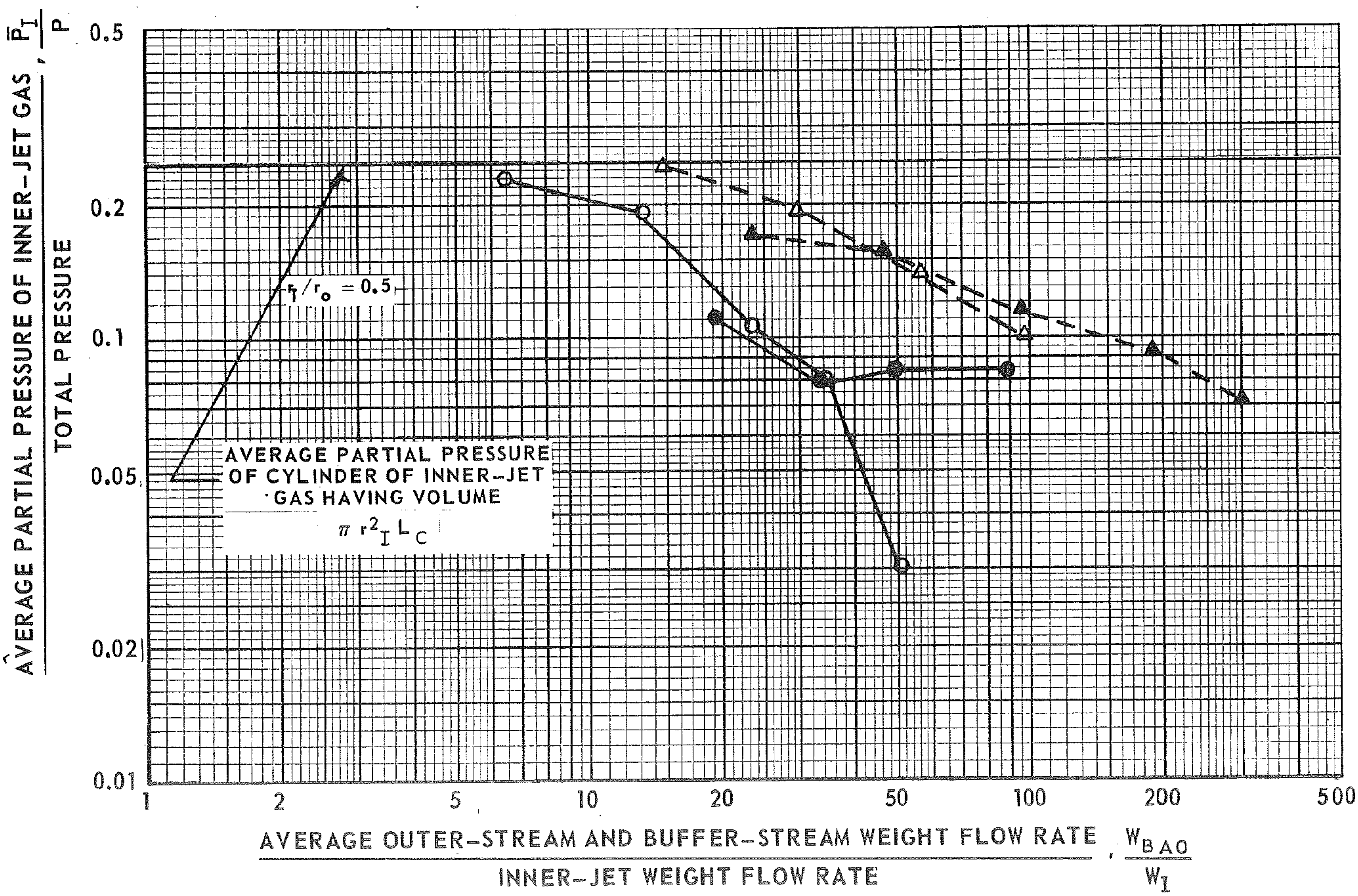

APPARENT COAXIAL JET CONTAINMENT WITH FOAM AND POROUS PLATE INLET

CONFIGURATION – SHORT CHAMBER AND FOAM AND INLET
WITH $r_I/r_O = 0.60$ AND $r_B/r_O = 0.73$

FLOW CONDITION – $V_{BAO} \approx 80$ FT/SEC, $V_B = 0$, OUTER-STREAM GAS-AIR

FLAGGED SYMBOL INDICATES DILUTION OF INNER-JET GAS DUE TO RECIRCULATION

SYMBOL	INNER-JET GAS
▲	FREON
△	AIR

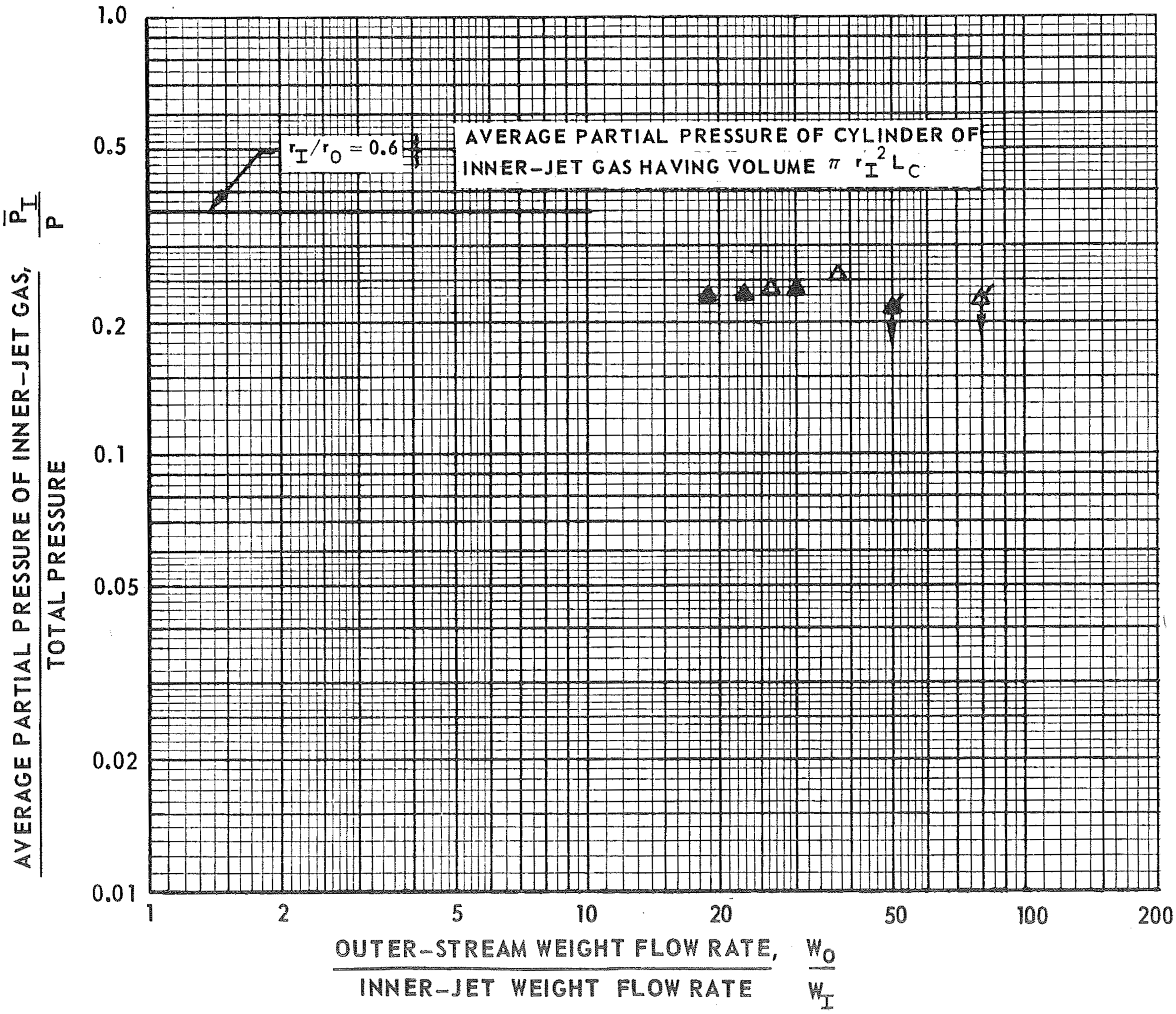

COMPARISON OF APPARENT COAXIAL-JET CONTAINMENT WITH FREON AS INNER-JET GAS FOR SEVERAL INLET CONFIGURATIONS

CONFIGURATION – SHORT CHAMBER

FLOW CONDITION – $V_{BAO} \approx 80$ FT/SEC, BUFFER AND OUTER GAS-AIR

FLAGGED SYMBOL INDICATES DILUTION OF INNER-JET GAS DUE TO RECIRCULATION OR RADIAL FLOW AT FOAM INLET

SYMBOL	INLET CONFIGURATION	r_I/r_O	r_B/r_O	DATA OBTAINED
○———○	a) SCREEN	0.50	0.65	REF. 3
△- - - - -△	b) FOAM	0.50	0.65	PHOTOGRAPHS
▲— — —▲	b) FOAM	0.60	0.73	PHOTOGRAPHS
■———■	c) FOAM AND PERFORATED PLATE	0.60	0.73	PHOTOGRAPHS

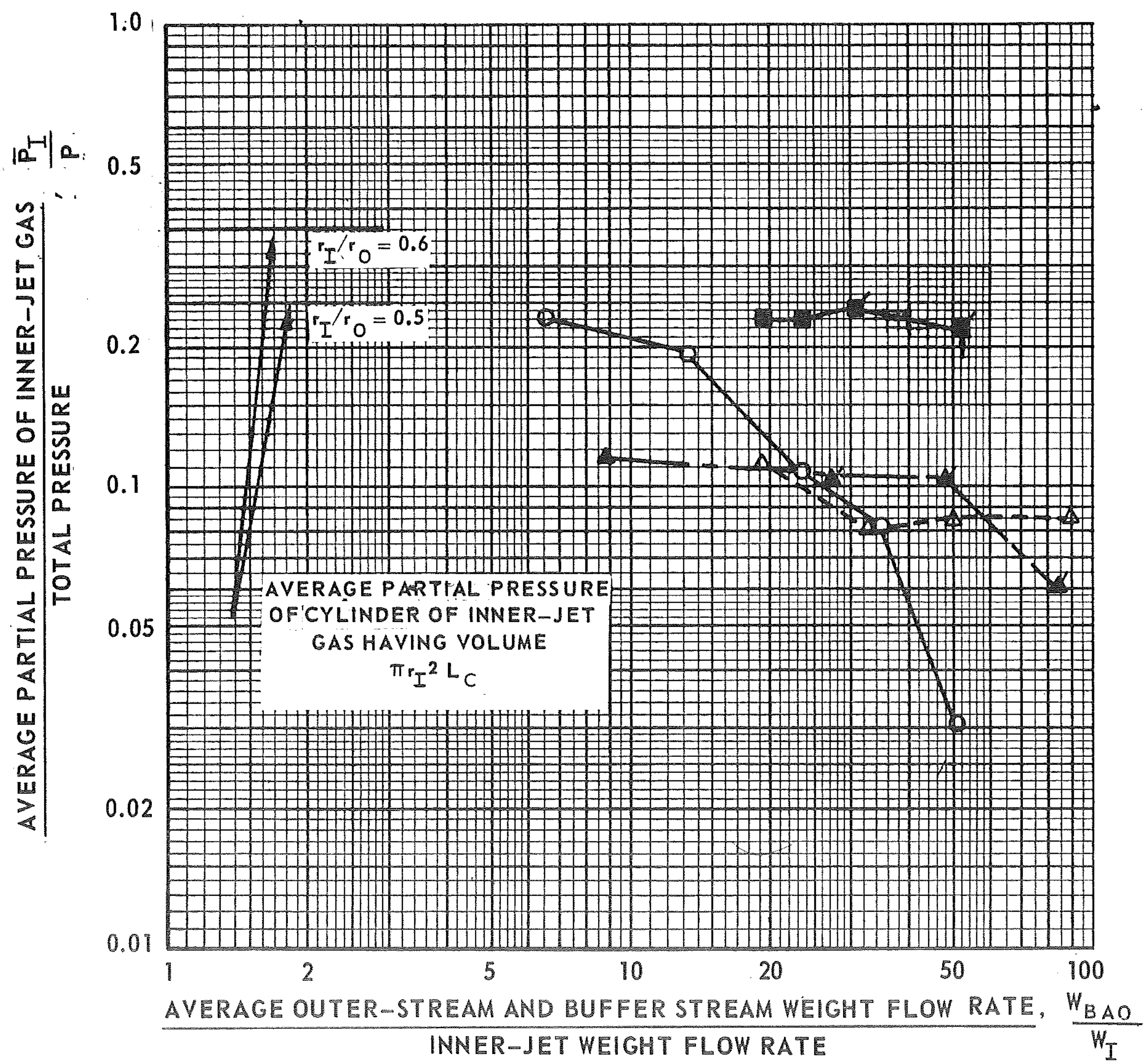

COMPARISON OF PRESENT AND PREVIOUS COAXIAL-JET CONTAINMENT WITH GNR OPEN CYCLE FLUID MECHANICS PERFORMANCE REQUIREMENTS

PERFORMANCE REGION AND REQUIREMENTS OBTAINED FROM REF. 2

FLAGGED SYMBOLS INDICATE DILUTION OF INNER-GAS DUE TO RECIRCULATION

SYMBOL	INNER-JET GAS	ρ_I/ρ_{BAO}	MEASUREMENT TECHNIQUE	WORK
△	AIR	1.0	LIGHT ABSORPTION TECHNIQUE	REF. 4
▲	FREON-II	4.7		
□	AIR	1.0	ESTIMATED FROM PHOTOGRAPHS	PRESENT REPORT
■	FREON-II	4.7		

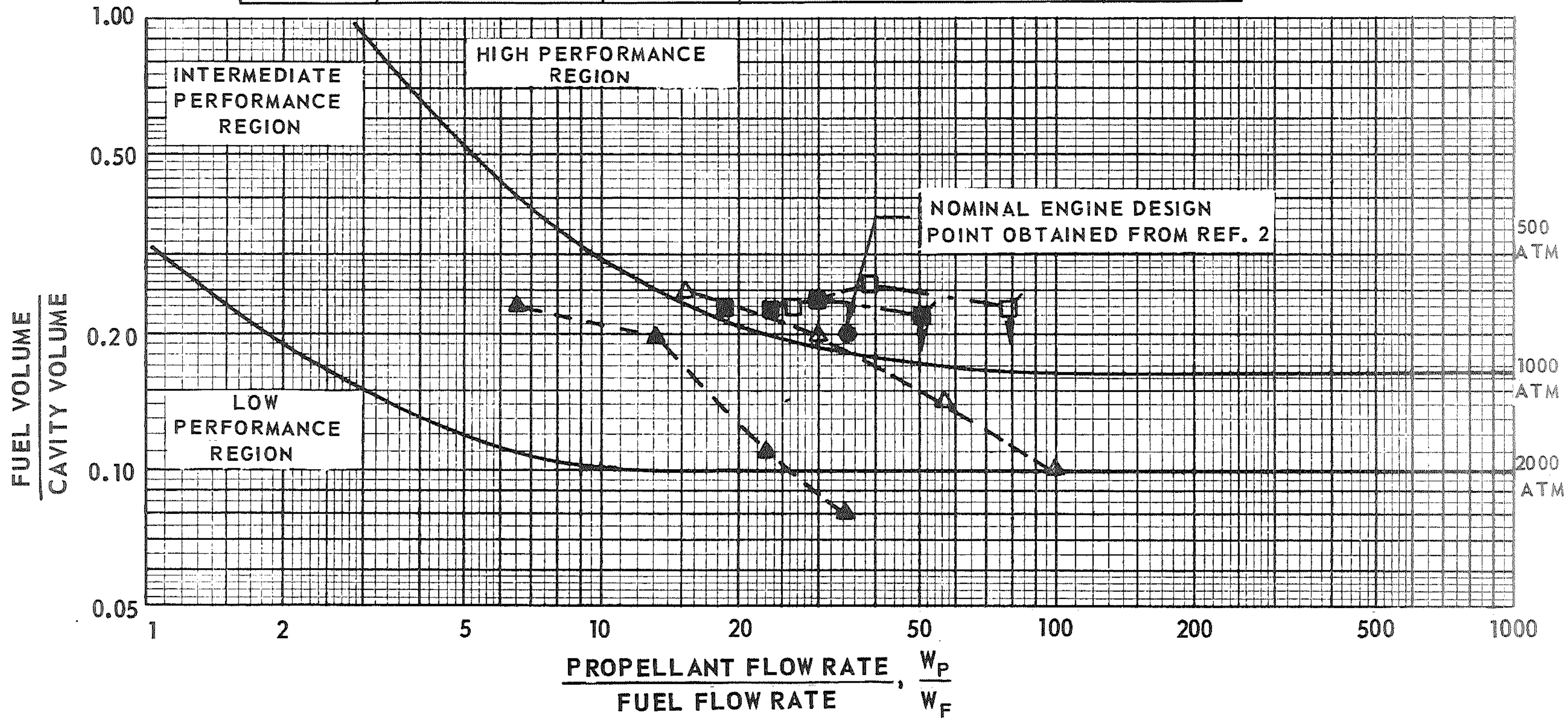

FIG. 25

UNITED AIRCRAFT CORPORATION